

---

**Research Articles: Cellular/Molecular**

## **PKD1 promotes functional synapse formation coordinated with N-cadherin in hippocampus**

**Cheng Cen<sup>1</sup>, Li-Da Luo<sup>1</sup>, Wen-Qi Li<sup>1</sup>, Gang Li<sup>1</sup>, Na-Xi Tian<sup>1</sup>, Ge Zheng<sup>1</sup>, Dong-Min Yin<sup>3</sup>, Yimin Zou<sup>4</sup> and Yun Wang<sup>1,2</sup>**

<sup>1</sup>Neuroscience Research Institute and Department of Neurobiology, School of Basic Medical Sciences, Key Laboratory for Neuroscience, Ministry of Education/National Health and Family Planning Commission, Peking University, Beijing 100191, China

<sup>2</sup>PKU-IDG/McGovern Institute for Brain Research, Peking University, Beijing 100871, China

<sup>3</sup>Key Laboratory of Brain Functional Genomics, Ministry of Education, Shanghai Key Laboratory of Brain Functional Genomics, School of Life Sciences, East China Normal University, Shanghai, China.

<sup>4</sup>Neurobiology Section, Biological Sciences Division, University of California, San Diego, La Jolla, California, USA.

DOI: 10.1523/JNEUROSCI.1640-17.2017

Received: 13 June 2017

Revised: 11 October 2017

Accepted: 7 November 2017

Published: 13 November 2017

---

**Author Contributions:** Y.W. conceived and directed the project. C.C. conducted the electrophysiological studies, the animal behavior studies and analyzed the data. L.D.L. conducted the cell culture experiments, the biochemical experiments and analyzed the data. W.Q.L., G.L., N.X.T., G.Z and D.M.Y. conducted some of the experiments and analyzed the data. C.C., L.D.L., D.M.Y., Y.Z. and Y.W. discussed the data. C.C., L.D.L. and Y.W. wrote the manuscript.

**Conflict of Interest:** The authors declare no competing financial interests.

This work was supported by grants from the National Natural Science Foundation of China (81600989 to C.C., 31530028 and 31720103908 to Y.W.), the Ministry of Science and Technology of China (2014CB542204 and 2015BAI08B02 to Y.W.) and China Postdoctoral Science Foundation (2015M580025 to C.C.). C.C. was supported in part by the Postdoctoral Fellowship of Peking-Tsinghua Center for Life Sciences. We thank Prof. Qihua He (Cell Analytical Laboratory, Medical and Healthy Analytical Center, Peking University) for technical support for imaging.

**Correspondence should be addressed to** Yun Wang, Neuroscience Research Institute and Department of Neurobiology, School of Basic Medical Sciences, Key Laboratory for Neuroscience, Ministry of Education/National Health and Family Planning Commission, Peking University, Beijing 100191, China. Email: [wangy66@bjmu.edu.cn](mailto:wangy66@bjmu.edu.cn)

**Cite as:** J. Neurosci ; 10.1523/JNEUROSCI.1640-17.2017

**Alerts:** Sign up at [www.jneurosci.org/cgi/alerts](http://www.jneurosci.org/cgi/alerts) to receive customized email alerts when the fully formatted version of this article is published.

Accepted manuscripts are peer-reviewed but have not been through the copyediting, formatting, or proofreading process.

---

1 **PKD1 promotes functional synapse formation coordinated with**  
2 **N-cadherin in hippocampus**

3 **Abbreviated title:** PKD1, N-cadherin and synapse formation

4 Cheng Cen (岑程)<sup>1\*</sup>, Li-Da Luo (罗丽达)<sup>1\*</sup>, Wen-Qi Li (李文琪)<sup>1</sup>, Gang Li (李刚)<sup>1</sup>,  
5 Na-Xi Tian (田纳西)<sup>1</sup>, Ge Zheng (郑歌)<sup>1</sup>, Dong-Min Yin (殷东敏)<sup>3</sup>, Yimin Zou (邹益  
6 民)<sup>4</sup>, Yun Wang (王韵)<sup>1,2</sup>

7 <sup>1</sup>Neuroscience Research Institute and Department of Neurobiology, School of Basic  
8 Medical Sciences, Key Laboratory for Neuroscience, Ministry of Education/National  
9 Health and Family Planning Commission, Peking University, Beijing 100191, China;

10 <sup>2</sup>PKU-IDG/McGovern Institute for Brain Research, Peking University, Beijing  
11 100871, China;

12 <sup>3</sup>Key Laboratory of Brain Functional Genomics, Ministry of Education, Shanghai Key  
13 Laboratory of Brain Functional Genomics, School of Life Sciences, East China  
14 Normal University, Shanghai, China.

15 <sup>4</sup>Neurobiology Section, Biological Sciences Division, University of California, San  
16 Diego, La Jolla, California, USA.

17 \*C.C. and L.D.L. contributed equally to this work.

18 Correspondence should be addressed to Yun Wang, Neuroscience Research Institute  
19 and Department of Neurobiology, School of Basic Medical Sciences, Key Laboratory  
20 for Neuroscience, Ministry of Education/National Health and Family Planning  
21 Commission, Peking University, Beijing 100191, China. Email:

22 [wangy66@bjmu.edu.cn](mailto:wangy66@bjmu.edu.cn)

---

23 Number of pages: 49

24 Number of figures: 10

25 Number of words: for Abstract, 183; for Introduction, 548; for Discussion, 756.

26 **Author Contributions:** Y.W. conceived and directed the project. C.C. conducted the  
27 electrophysiological studies, the animal behavior studies and analyzed the data. L.D.L.  
28 conducted the cell culture experiments, the biochemical experiments and analyzed the  
29 data. W.Q.L., G.L., N.X.T., G.Z and D.M.Y. conducted some of the experiments and  
30 analyzed the data. C.C., L.D.L., D.M.Y., Y.Z. and Y.W. discussed the data. C.C.,  
31 L.D.L. and Y.W. wrote the manuscript.

32 **Acknowledgments:** This work was supported by grants from the National Natural  
33 Science Foundation of China (81600989 to C.C., 31530028 and 31720103908 to  
34 Y.W.), the Ministry of Science and Technology of China (2014CB542204 and  
35 2015BAI08B02 to Y.W.) and China Postdoctoral Science Foundation (2015M580025  
36 to C.C.). C.C. was supported in part by the Postdoctoral Fellowship of  
37 Peking-Tsinghua Center for Life Sciences. We thank Prof. Qihua He (Cell Analytical  
38 Laboratory, Medical and Healthy Analytical Center, Peking University) for technical  
39 support for imaging.

40 **Competing Interests:** The authors declare no competing financial interests.

41

---

42 **Abstract**

43 Functional synapse formation is critical for the wiring of neural circuits in the  
44 developing brain. The cell adhesion molecule N-cadherin plays important roles in  
45 target recognition and synaptogenesis. However, the molecular mechanisms that  
46 regulate the localization of N-cadherin and the subsequent effects remain poorly  
47 understood. Here, we show that protein kinase D1 (PKD1) directly binds to  
48 N-cadherin at amino acid residues 836-871 and phosphorylates it at Ser 869, 871, 872,  
49 thereby increasing the surface localization of N-cadherin and promoting functional  
50 synapse formation in primary cultured hippocampal neurons obtained from embryonic  
51 day 18 rat embryos of either sex. Intriguingly, neuronal activity enhances the  
52 interactions between N-cadherin and PKD1, which are critical for the  
53 activity-dependent growth of dendritic spines. Accordingly, either disruption the  
54 binding between N-cadherin and PKD1 or preventing the phosphorylation of  
55 N-cadherin by PKD1 in the hippocampal CA1 region of male rat leads to the  
56 reduction in synapse number and impairment of long-term potentiation (LTP).  
57 Together, this study demonstrates a novel mechanism of PKD1 regulating the surface  
58 localization of N-cadherin and suggests that the PKD1-N-cadherin interaction is  
59 critical for synapse formation and function.

60

61 **Significance Statement**

62 Defects in synapse formation and function lead to various neurological diseases, while  
63 the mechanisms underlying the regulation of synapse development are far from clear.

---

64 Our results suggest that protein kinase D1 (PKD1) functions upstream of N-cadherin,  
65 a classical synaptic adhesion molecule, to promote functional synapse formation.  
66 Notably, we identified a crucial binding fragment to PKD1 at C-terminus of  
67 N-cadherin, and this fragment also contains PKD1 phosphorylation sites. Through this  
68 interaction, PKD1 enhances the stability of N-cadherin on cell membrane and  
69 promotes synapse morphogenesis and synaptic plasticity in an activity-dependent  
70 manner. Our study reveals the role of PKD1 and the potential downstream mechanism  
71 in synapse development, and contributes to the research for neurodevelopment and the  
72 therapy for neurological diseases.

73

#### 74 **Introduction**

75 Brain function relies on the establishment and organization of proper neuronal  
76 circuitry consisting of a vast but sophisticated interconnected network of synapses.  
77 Synapses are specialized asymmetrical connections between neurons that function in  
78 information processing and integration. Synapse formation, elimination and  
79 remodeling are essential for the development of neural circuits and cognitive  
80 functions such as learning and memory (Kandel et al., 2014). Cell adhesion molecules  
81 (CAMs), which can align the presynaptic active zone and the postsynaptic density  
82 across the synaptic cleft, have been intensively studied for their important roles in  
83 neurite outgrowth, neuronal polarity, neuronal migration, synapse formation and  
84 synaptic plasticity both in the developing and mature brain (Togashi et al., 2002;  
85 Arikath and Reichardt, 2008; Seong et al., 2015).

---

86 N-cadherin, one of the important CAMs in nervous system, is a type I classical  
87 cadherin that is widely expressed in both pre- and postsynaptic membranes of  
88 excitatory neurons in mammals (Arikkath and Reichardt, 2008). N-cadherin mediates  
89 calcium-dependent, homophilic interactions across the synaptic cleft, and plays  
90 crucial roles in dendrite morphogenesis, synapse formation, synaptic plasticity and  
91 neural disorders associated with autism, bipolar disease, schizophrenia and  
92 Alzheimer's disease (Schrick et al., 2007; Bacchelli et al., 2014; Tucci et al., 2014;  
93 Uribe-Arias et al., 2016). Although the functions of N-cadherin in neurons have been  
94 extensively investigated, the post-translational modification and regulation of the  
95 membrane localization of N-cadherin have been rarely studied.

96 Protein kinase D (PKD) is a serine/threonine protein kinase family that includes three  
97 kinase isoforms: PKD1, PKD2 and PKD3 (Johannes et al., 1994). PKDs are activated  
98 by a novel PKC family and are recruited to the plasma membrane or to intracellular  
99 membranes through binding DAG (diacylglycerol) to achieve full activation  
100 (Valverde et al., 1994; Iglesias and Rozengurt, 1998; Iglesias et al., 1998). PKDs have  
101 been studied for their roles in diverse cellular functions including cell proliferation  
102 and migration, gene expression, cell motility and adhesion (Rozengurt, 2011). In the  
103 nervous system, PKDs have been shown to regulate Golgi functions, neuronal polarity,  
104 dendrite development, synaptic plasticity and memory formation (Bisbal et al., 2008;  
105 Yin et al., 2008; Czondor et al., 2009; Avriyanti et al., 2015; Bencsik et al., 2015). It  
106 has been reported that PKD1 can bind to and phosphorylate epithelial-type cadherin  
107 (E-cadherin) and thus regulate the adhesion of cancer cells (Jaggi et al., 2005). Based

---

108 on the observations that N-cadherin shares a similar structure and a highly conserved  
109 cytoplasmic domain with E-cadherin (Gumbiner, 2005), we proposed that N-cadherin  
110 might contribute to the “cell-cell adhesion” between neurons under regulation of  
111 PKD1.

112 In this work, we used morphological and electrophysiological studies of cultured  
113 hippocampal neurons to demonstrate that PKD1 promotes functional synapse  
114 formation by acting upstream of N-cadherin. We found that PKD1 directly binds to  
115 N-cadherin at amino acid residues 836-871 and phosphorylates N-cadherin at Ser 869,  
116 871, 872, leading to increased membrane localization of N-cadherin. Furthermore, we  
117 demonstrated that disruption of the interaction between PKD1 and N-cadherin reduces  
118 the surface localization of N-cadherin and thus inhibits functional synapse formation  
119 and long-term potentiation (LTP). We also demonstrated that neural activity enhances  
120 the interaction between N-cadherin and PKD1 and that neural activity-driven spine  
121 growth requires the kinase activity of PKD1. This study identifies N-cadherin as a  
122 novel synaptic substrate of PKD1 and demonstrates the pivotal roles of these proteins  
123 in synaptogenesis and in synaptic plasticity.

124

## 125 **Materials and Methods**

### 126 **Animals**

127 Sprague-Dawley (SD) rats were housed in a temperature- ( $23\pm 2^\circ\text{C}$ ) and humidity-  
128 ( $50\pm 5\%$ ) controlled environment. The animals were maintained on a 12-h light and  
129 dark cycle with food and water ad libitum. All animal studies were approved by the

---

130 Animal Center of the Peking University Health Science Center, and the experiments  
131 were carried out in accordance with the relevant guidelines, including any relevant  
132 details.

133

134

#### 135 **DNA Constructs and Chemicals**

136 Human PKD1 (h-PKD1) cDNA was cloned into the mammalian expression vector  
137 pcDNA3.1 to produce a his-myc-tagged expression plasmid. DN-hPKD1  
138 (D727A-hPKD1) and rat-hPKD1 were generated by site-directed mutagenesis using  
139 PCR. Rat N-cadherin plasmid with myc tag (N-cad) was kindly provided by Prof.  
140 Tanaka (Osaka University, Suita, Osaka, Japan). N-cad $\Delta$ 836-871 (N-cadherin with a  
141 deletion of amino acids of 836-871) and N-cad mut (N-cadherin with S869A, S871A  
142 and S872A) were generated by PCR. GFP-hPKD1 and related mutants were  
143 constructed as previously described (Wang et al., 2004; Yin et al., 2008). shRNAs  
144 co-expressing EGFP against rat PKD1 and N-cadherin (shPKD1 and shN-cad) were  
145 purchased from Shanghai Genechem. The target mRNA sequences were as follows:  
146 for PKD1, 5'-GGUUCUGGACAGUUCGGAA-3'; and for N-cadherin,  
147 5'-GACUGGAUUUCCUGAAGAU-3' (Zhang et al., 2010; Lewallen et al., 2011).  
148 shRNA targeting a nonspecific sequence (shGFP) was used as a control. Endogenous  
149 rat PKD1 and transfected rat-hPKD1 can be knocked down by shPKD1, whereas  
150 transfected hPKD1 resists shPKD1.

151 To prepare constructs for protein purification, PKD1, cytoplasmic N-cadherin and

---

152 various constructs were cloned into the pGEX-5X-1 vector with an N-terminal  
153 glutathione-S-transferase (GST) tag or into the pET-28a(+) vector with an N-terminal  
154 His6 tag.

155 Two pairs of interfering peptides were created and used in the experiments. Fusion  
156 with the TAT protein sequence (RKKRRQRRR) renders the peptides cell-permeable.  
157 TAT-836-871, which was used to disrupt the binding of PKD1 to N-cadherin, consists  
158 of the TAT sequence and amino acids 836-871 of N-cadherin, the region through  
159 which N-cadherin binds to PKD1 (the sequence was  
160 RKKRRQRRR-INEGLKAADNDPTAPPYDSLIVFDYEGSGSTAGSLS). As a  
161 control peptide, amino acids 836-871 of N-cadherin were replaced with a scrambled  
162 sequence of the same 36 amino acids (termed TAT-scramble, the sequence was  
163 RKKRRQRRR-LPTALGLSLYKSFPGYDGSVISDGEDAPDAASNNT). TAT-S3,  
164 which was used to disrupt the phosphorylation of N-cadherin by PKD1, consists of  
165 the TAT sequence and amino acids 865-878 of N-cadherin, including the three  
166 phosphorylation sites, Ser 869, 871, 872 (the sequence was  
167 RKKRRQRRR-STAGSLSSLNSSSS). As a control peptide, Ser 869, 871, 872 were  
168 replaced with alanine in the peptide TAT-S3A (the sequence was  
169 RKKRRQRRR-STAGALAALNSSSS). For neuronal morphology analysis, 3  $\mu$ M  
170 peptide was added to the medium at days *in vitro* (DIV) 10 after GFP transfection at  
171 DIV8. For electrophysiological recording, 3  $\mu$ M peptides were added to the medium  
172 without transfection. The TAT fusion peptides were synthesized by GL Biochem  
173 (Shanghai, China). The mass and purity of the peptides were verified by HPLC.

---

174 To study the role of PKD1 in neural activity-induced spine growth, 12 mM KCl  
175 (Sigma Aldrich) was added to the culture medium to increase neural activity. For  
176 biochemical experiments, KCl was added at DIV6 or 7, and cortical neurons were  
177 harvested 12 h later. For morphological experiments, KCl was added at DIV10 (2 d  
178 after transfection) and maintained until hippocampal neurons were fixed at DIV15.  
179 Gö6976 (Calbiochem), Bim (Calbiochem) and PMA (Sigma Aldrich) were diluted in  
180 DMSO (Sigma Aldrich) for use.

181

#### 182 **Cell Culture and Transfection**

183 Hippocampal and cortical neurons were obtained from embryonic day 18 rat embryos  
184 of either sex and plated onto 35-mm dishes coated with poly-D-lysine (Sigma Aldrich)  
185 at an appropriate density. After 4 h in plating media (10% fetal bovine serum in  
186 DMEM), the cultures were transferred to neurobasal medium supplemented with 2%  
187 B27 and 0.5 mM GlutaMAX-I (Gibco Invitrogen). Half of the medium was replaced  
188 with fresh medium every 3 days. At DIV 3, cytosine arabinoside was added to the  
189 maintenance medium at a final concentration of 10  $\mu$ M to inhibit glial proliferation.  
190 For most morphological and electrophysiological experiments, hippocampal neurons  
191 at DIV8 were transfected with 3  $\mu$ g of the indicated PKD1/N-cadherin constructs  
192 together with 1  $\mu$ g GFP-expressing plasmid (pEGFP-N1) or shRNAs co-expressing  
193 EGFP to label entire neurons using Lipofectamine-2000 (Invitrogen) following the  
194 manufacturer's guidelines. For the biochemical experiments, cortical neurons were  
195 primarily used.

---

196 Mouse N2a and rat C6 cells were maintained in DMEM supplemented with 10% fetal  
197 bovine serum. The cells were transfected with Lipofectamine-2000 (Invitrogen)  
198 according to the manufacturer's instructions.

199

#### 200 **Western Blots**

201 Western blotting experiments were performed according to previously described  
202 protocols (Xing et al., 2012). The antibodies used in Western blots were rabbit  
203 polyclonal anti-PKD1 (sc-639; Santa Cruz Biotechnology), rat monoclonal  
204 anti-N-cadherin MNCD2 (Developmental Studies Hybridoma Bank, DSHB), mouse  
205 monoclonal anti-N-cadherin 3B9 (Invitrogen), mouse monoclonal anti-myc (TA-01;  
206 Origene), mouse monoclonal anti- $\beta$ -catenin (BD), mouse monoclonal anti-GST  
207 (Applygen), mouse monoclonal anti-His (Applygen), mouse monoclonal anti-human  
208 Tfr (Invitrogen), mouse monoclonal anti-GFP (Santa Cruz Biotechnology) and mouse  
209 monoclonal anti- $\beta$ -actin (TA-09; Origene) followed by horseradish  
210 peroxidase-conjugated secondary antibodies (Sigma Aldrich & Origene).

211

#### 212 **Pull-down Assay**

213 GST-fusion proteins were expressed in *Escherichia coli* BL21 (DE3) cells and  
214 purified using Glutathione Sepharose<sup>TM</sup> 4 Fast Flow (Amersham Pharmacia)  
215 according to the manufacturer's instructions; His6-fusion proteins were purified using  
216 Ni-NTA agarose beads (QIAGEN) following the manufacturer's instructions. For  
217 binding assays, eluted His6-fusion protein was incubated with immobilized GST (as a

---

218 control) or with GST-fusion protein for 2 h at 4°C. The mixture was then washed,  
219 eluted and subjected to Western blot analysis.

220

### 221 **Immunoprecipitation**

222 Protein extracts from transfected cells, neurons or rat hippocampal tissues were  
223 prepared as for Western blots. Extracts containing 400-500 µg of protein were  
224 incubated with antibodies against PKD1 (1:50) or N-cadherin 3B9 (1:50) at 4°C for 3  
225 h prior to incubation with protein A-Sepharose CL-4B resin (GE Healthcare)  
226 overnight. The immunoprecipitates were washed six times with 0.1% Triton X-100 in  
227 TBS. The final pellets were boiled in SDS-PAGE sample buffer and subjected to  
228 Western blot analysis.

229

### 230 **Cell Surface Biotinylation Assay**

231 Cell cultures were washed with ice-cold PBS (pH 8.0) and then incubated for 45 min  
232 at 4°C with EZ-Link Sulfo-NHS-SS-biotin (Pierce) to biotinylation surface proteins.  
233 After quenching with PBS containing 100 mM glycine and washing with PBS (pH  
234 7.4), the cells were lysed with RIPA lysis buffer (1% Triton X-100 and 0.1% SDS in  
235 TBS). The supernatants from the cell lysates were incubated with Ultralink Plus  
236 immobilized streptavidin beads (Pierce) overnight at 4°C to capture biotinylated  
237 surface proteins. After washing the beads six times with RIPA buffer, the bound  
238 proteins were eluted by boiling for 5 min with SDS-PAGE sample buffer and were  
239 analyzed by Western blot.

240

241 ***In Vitro* Kinase Assay**

242 The phosphorylation of N-cadherin by PKD1 under various treatments was assessed  
243 following immunoprecipitation. Extracts containing 150 µg of protein obtained from  
244 lysates of young hippocampal neurons treated with Gö6976, Bim, PMA or control  
245 solvent (DMSO) were incubated with an antibody against PKD1 (1:100) or with  
246 normal rabbit IgG (sc-2027, Santa Cruz Biotechnology) as a control to  
247 immunoprecipitate PKD1 at 4°C for 3 h before overnight incubation with protein  
248 A-Sepharose CL-4B resin. After successively washing with lysis buffer and assay  
249 buffer (30 mM Tris, pH 7.6, 10 mM MgCl<sub>2</sub> and 1 mM dithiothreitol), the final pellets  
250 were resuspended to a final volume of 25 µl in assay buffer. To initiate the  
251 phosphorylation reaction, 10 µl of phosphorylation mix (assay buffer containing 5 µCi  
252 [ $\gamma$ -<sup>32</sup>P]ATP) was added. The mixture was incubated at 30 °C for 30 min, and the  
253 reaction was terminated by the addition of SDS-PAGE sample buffer. After boiling for  
254 5 min, the samples were subjected to SDS-PAGE. The gels were stained with  
255 Coomassie Brilliant Blue, dried, and exposed to x-ray film for autoradiography.  
256 To detect the potential sites of phosphorylation in N-cadherin by PKD1, purified  
257 His6-N-cadherin c-ter protein and various constructs were respectively mixed with  
258 commercial purified PKD1 (Merck Millipore) in assay buffer in a final volume of 25  
259 µl, and kinase assays were conducted as described above.

260

261 **Immunostaining**

---

262 For analysis of PKD1 distribution in neurons, cultured hippocampal neurons were  
263 fixed at DIV15 by 4% paraformaldehyde and 4% sucrose in PBS for 20 min at room  
264 temperature, followed by 1 h blocking solution with 3% bovine serum albumin (BSA)  
265 and 0.3% Triton X-100 in PBS. Incubation with primary antibodies and secondary  
266 antibodies were done in the blocking buffer (1% BSA and 0.3% Triton X-100 in PBS)  
267 at 4°C overnight respectively. Finally, the cells were mounted on slides, and the  
268 stained sections were examined using a Leica SP8 confocal laser scanning microscope  
269 at 63X (NA 1.4) objective at 0.75X and 4X zoom. Antibodies used in immunostaining  
270 are rabbit polyclonal anti-PKD1 (sc-639; Santa Cruz Biotechnology) and mouse  
271 monoclonal anti-N-cadherin 3B9 (Invitrogen) followed by Alexa Fluro-488 goat  
272 anti-rabbit IgG (Invitrogen) and Alexa Fluro-594 donkey anti-mouse IgG (Invitrogen).

273

#### 274 **PSD Preparations**

275 Cytosol, synaptosome, synaptosomal membrane and PSD fractions from the  
276 hippocampal CA1 region of rat brain were prepared using the previously described  
277 procedure with slight modifications (Carlin et al., 1980; Cho et al., 1992; Yang et al.,  
278 2015). In brief, CA1 region of hippocampus were homogenized on ice using 20  
279 strokes of a Teflon-glass homogenizer in 1 ml of HEPES-buffered sucrose (0.32 M  
280 sucrose, 4 mM HEPES, pH7.4) containing freshly added protease inhibitors, then  
281 centrifuged at 800~1000× g at 4 °C to remove the pelleted nuclear fraction (P1).  
282 Supernatant (S1) was centrifuged at 10000× g for 15 min to yield the crude  
283 synaptosomal pellet (P2) and pellet was washed once in 1 ml HEPES-buffered

---

284 sucrose. P2 was lysed by hypoosmotic shock in 900  $\mu$ l ice-cold 4 mM HEPES, pH 7.4  
285 plus protease inhibitors, homogenized by pipetting and mixed for 30 min at 4 °C. The  
286 lysate was centrifuged at 25000 $\times$  g for 20 min to yield supernatant (S3, crude synaptic  
287 vesicle fraction) and pellet (P3, lysed synaptosomal membrane fraction). To prepare  
288 the PSD fraction, P3 was resuspended in 900  $\mu$ l of ice-cold 50 mM HEPES, pH 7.4, 2  
289 mM EDTA, plus protease inhibitors and 0.5% Triton X-100, rotated for 15 min at  
290 4 °C and centrifuged at 32000 $\times$  g for 20 min to obtain the PSD pellet. PSD pellets  
291 were resuspended in 50  $\mu$ l ice-cold 50 mM HEPES, pH 7.4, 2 mM EDTA plus  
292 protease inhibitors.

293

#### 294 **Analysis of Neuronal Morphology**

295 Dissociated hippocampal neurons grown at low density were used to determine the  
296 morphological characteristics of the neurons. Hippocampal neurons were fixed at  
297 DIV15 in 4% paraformaldehyde and 4% sucrose in PBS for 20 min at room  
298 temperature, mounted on slides, and imaged using an Olympus confocal laser  
299 scanning microscope (FV1000) with a 60X (NA 1.42) objective at 3X zoom. Spine  
300 stacks were acquired at 0.35- $\mu$ m z-intervals to image the entire thickness of the  
301 dendrite. Measurement and analysis of the images were performed using Image Pro  
302 Plus (Media Cybernetics). Protrusions whose length exceeds twice the value of its  
303 width are considered as filopodia and the rest are spines. Spine density, protrusion  
304 density and filopodia density are presented as average numbers per 10  $\mu$ m of  
305 dendrites. For spine area, protrusion area, protrusion width and protrusion length, the

---

306 experimental groups were normalized to the control groups. Representative images  
307 were imaged using a Leica SP8 confocal laser scanning microscope with a 63X (NA  
308 1.4) objective at 0.75X and 4X zoom.

309

### 310 **Whole-cell Recordings on Cultured Neurons**

311 E18 rat hippocampal neurons were cultured *in vitro* for 10-12 d. Whole-cell  
312 patch-clamp recordings were carried out at room temperature using a HEKA EPC9  
313 amplifier (HEKA Elektronik, Lambrecht, Germany) and low-resistance pipettes (3–5  
314 M $\Omega$ ). The pipettes for whole-cell recordings were pulled (P-97, Sutter Instruments,  
315 Novato, CA) using borosilicate glass capillaries (1.5 mm OD, 0.84 mm ID; VitalSense  
316 Scientific Instruments Co., Ltd, Wuhan, China). The intracellular solutions contained  
317 (in mM) 110 K-gluconate, 20 KCl, 5 MgCl<sub>2</sub>, 20 HEPES, 0.6 EGTA, 2 Mg-ATP and  
318 0.2 Na-GTP (pH = 7.3, 300 mOsm). The extracellular solution contained (in mM) 129  
319 NaCl, 5 KCl, 30 glucose, 25 HEPES, 2 CaCl<sub>2</sub>, 1 MgCl<sub>2</sub>, 0.001 tetrodotoxin (TTX),  
320 0.001 strychnine and 0.02 bicuculline (pH = 7.3, 315 mOsm). For miniature  
321 excitatory postsynaptic currents (mEPSCs) recordings, neurons were voltage-clamped  
322 at -60 mV, and data were sampled at 10 kHz and filtered at 2 kHz. Neurons with a  
323 resting potential of at least -60 mV and an  $R_{series}$  that fluctuated within 15% of the  
324 initial value (< 20 M $\Omega$ ) were analyzed. The total recording duration for each neuron  
325 was 250 s. Data analysis was performed blind using MiniAnalysis software  
326 (Synptosoft) offline. The frequency and amplitude of mEPSCs were compared using  
327 Student's *t*-test or one-way ANOVA with Bonferroni's post-hoc test.  $P < 0.05$  was

---

328 considered to be statistically significant. Data are presented as mean  $\pm$  SEM.

329

330 **Stereotactic Injection (Intrahippocampal Injection)**

331 Stereotaxic surgery was performed under anesthesia with 10% chloral hydrate (m/v,  
332 i.p.). Peptides were bilaterally injected into the hippocampal CA1 region of rats using  
333 a microinfusion pump (CMA 100; CMA Microdialysis, Stockholm, Sweden). The  
334 coordinates used to target the CA1 region of hippocampus were based on the  
335 stereotaxic atlas of Paxinos and Watson (1986): anterior/posterior -3.8 mm,  
336 medial/lateral  $\pm$ 2.5 mm and dorsal/ventral -2.8 mm. Peptides were dissolved in saline  
337 to a concentration of 20  $\mu$ g/ $\mu$ l, and 0.5  $\mu$ l peptide per side was infused over 3 min  
338 followed by 2 additional min to allow diffusion before withdrawal. The injection of  
339 peptides was performed 12 h prior to slice preparation and electrophysiological  
340 recording.

341

342 **Brain Slice Preparation and Electrophysiological Recording**

343 Three- to four-week-old rats were anesthetized with 10% chloral hydrate (m/v, i.p.).  
344 Brains were quickly removed and submerged in ice-cold sucrose-replaced artificial  
345 cerebrospinal fluid (ACSF) dissection solution containing (in mM) 10 glucose, 213  
346 sucrose, 3 KCl, 1 NaH<sub>2</sub>PO<sub>4</sub>, 26 NaHCO<sub>3</sub>, 0.5 CaCl<sub>2</sub>, 5 MgCl<sub>2</sub>, pH = 7.4, 315 mOsm  
347 (saturated with 95% O<sub>2</sub> - 5% CO<sub>2</sub>). Acute hippocampal slices (300  $\mu$ m) were prepared  
348 using a Leica VT1000S vibratome. After dissection, slices were incubated at 33°C for  
349 at least 1 h in ACSF containing (in mM) 10 glucose, 125 NaCl, 5 KCl, 1.2 NaH<sub>2</sub>PO<sub>4</sub>,

---

350 26 NaHCO<sub>3</sub>, 2.6 CaCl<sub>2</sub>, 1.3 MgCl<sub>2</sub> (saturated with 95% O<sub>2</sub> - 5% CO<sub>2</sub>) and 100 μM  
351 picrotoxin, pH = 7.4, 315 mOsm. A single slice was then transferred to a recording  
352 chamber and submerged beneath continuously perfusing oxygenated ACSF. The  
353 chamber was perfused at a speed of 2 ml/min.

354 Field excitatory postsynaptic potentials (fEPSPs) were recorded in the stratum  
355 radiatum of CA1 with a patch pipette (1-2 MΩ) filled with ACSF. A bipolar tungsten  
356 stimulating electrode (FHC) was placed in the Schaffer collaterals to deliver test and  
357 conditioning stimuli. Test stimuli were delivered at 0.05 Hz with an intensity adjusted  
358 to elicit a fEPSP amplitude 40%-50% of maximum as the baseline. After obtaining a  
359 stable baseline for 20 min, LTP was induced by 4 consecutive trains (1 s) of stimuli at  
360 100 Hz (HFS) separated by 20 s using the same stimulus strength as in baseline  
361 recording. LTP values were recorded for another 60 min at 0.05 Hz after HFS  
362 induction. The initial slope of the response was used to assess changes in synaptic  
363 strength. Paired-pulse responses were recorded at 50-ms, 100-ms, 150-ms, 200-ms,  
364 250-ms, and 300-ms inter-stimulus intervals. The facilitation ratio was calculated as  
365 fEPSP2 slope/fEPSP1 slope.

366 The field EPSP was recorded using a HEKA EPC10 amplifier (HEKA Elektronik,  
367 Lambrecht, Germany) and PatchMaster software (HEKA Elektronik). The data were  
368 sampled at 10 kHz and filtered at 2 kHz. Statistical analysis was performed using Igor  
369 software (Wavemetrics) and Graph Pad Prism 5. Two-way ANOVA with Bonferroni's  
370 post-hoc test and Student's *t*-test were used to determine the statistical significance of  
371 the data.  $P < 0.05$  was considered to be statistically significant. Data are presented as

---

372 mean  $\pm$  SEM.

373

#### 374 **Experimental Design and Statistical Analysis**

375 Morphological and electrophysiological studies on primary cultured hippocampal  
376 neurons or brain slices were conducted to explore the function of PKD1 and  
377 PKD1-N-cadherin interaction. Biochemical studies on primary cultured cortical  
378 neurons etc. were conducted to explore the detailed mechanism.

379 Statistical analysis was performed using Prism 5.0 (Graph Pad Software).

380 Comparisons between groups were performed using Student's *t*-test, one-way  
381 ANOVA followed by Bonferroni's post-hoc test, or two-way ANOVA followed by  
382 Bonferroni's post-hoc test. All data are presented as mean  $\pm$  SEM.

383

384

#### 385 **Results**

##### 386 **N-cadherin directly interacts with PKD1**

387 Considering that PKD1 binds to and phosphorylates E-cadherin in LNCaP prostate  
388 cancer cells (Jaggi et al., 2005), we speculated that there might be a comparable link  
389 between PKD1 and N-cadherin in nervous system. The GST pull-down assay verified  
390 our speculation that PKD1 could directly interact with N-cadherin (Fig. 1A). The  
391 immunoprecipitated PKD1 from the rat brain with PKD1 antibody was used in the *in*  
392 *vitro* kinase assay and N-cad-C-ter was phosphorylated by the immunoprecipitated  
393 PKD1 (Fig. 1B, left). This phosphorylation level of N-cad-C-ter was reduced in the

---

394 presence of the PKD1 inhibitor Gö6976 and the PKC inhibitor BIM, and increased by  
395 the application of the PKC activator PMA (Fig. 1B, right). The amount of the  
396 immunoprecipitated PKD1 was represented by IgG bands (the Coomassie staining  
397 IgG bands) (Fig. 1B, right). These results support our hypothesis that PKD1 can bind  
398 to and phosphorylate N-cadherin. To determine the subcellular distribution of PKD1,  
399 we performed the PSD preparation experiments on hippocampal CA1 region of  
400 postnatal 3~4 week old rats. Subcellular fractionation assays revealed that a  
401 significant amount of PKD1 was distributed in the PSD fraction (Fig. 1C), which  
402 suggested that PKD1 is mainly presented and interacts with N-cadherin in the  
403 postsynaptic compartment. Moreover, Immunofluorescence staining showed that  
404 PKD1 co-localized with N-cadherin partially at dendritic spines of hippocampal  
405 neurons (Fig. 1D). These results demonstrated that PKD1 co-localizes with  
406 N-cadherin at dendritic spines mainly in the postsynaptic compartment and might  
407 regulate N-cadherin in the nervous system.

408 **PKD1 promotes synapse formation and function by acting upstream of**  
409 **N-cadherin**

410 N-cadherin has been shown to play important roles in synapse formation and synaptic  
411 plasticity (Bozdagi et al., 2000; Friedman et al., 2015; Seong et al., 2015). Combined  
412 with the observations above, we first used *in vitro* cultured hippocampal neurons to  
413 examine the potential functions of PKD1 in synapse formation and function. The  
414 cultured neurons were transfected at DIV 8 with various PKD1 constructs along with  
415 GFP to show the morphology of dendritic spines where most excitatory synapses are

---

416 formed. The density and morphology of spines were analyzed at DIV 15, the time at  
417 which the majority of the protrusions have developed into mature spines (Yoshimura  
418 et al., 2006; Tahirovic and Bradke, 2009). Overexpression of wild-type human PKD1  
419 (hPKD1) increased the spine density ( $p < 0.0001$ ,  $F_{(2,49)} = 47.25$ , one-way ANOVA)  
420 and spine area ( $p < 0.0001$ ,  $F_{(2,49)} = 149.8$ , one-way ANOVA) compared to the empty  
421 vector, suggesting that PKD1 promotes spine formation (Fig. 2A). To confirm  
422 whether a correlation exists between the observed changes in spine morphology and  
423 synaptic transmission, we performed whole-cell patch-clamp recordings of mEPSCs  
424 in neurons to measure their basal synaptic properties. We found that overexpression of  
425 hPKD1 significantly increased mEPSC frequency ( $p < 0.0001$ ,  $F_{(2,28)} = 20.53$ ,  
426 one-way ANOVA) but did not affect mEPSC amplitude ( $p = 0.6167$ ,  $F_{(2,28)} = 0.4918$ ,  
427 one-way ANOVA) (Fig. 2B), indicating that a greater number of functional synapses  
428 were formed after hPKD1 overexpression.

429 As a serine/threonine kinase, the activity of endogenous PKD1 changes in parallel  
430 with neuronal maturation. By using an antibody recognizing autophosphorylated  
431 human PKD1, Czöndör *et al.* reported that the relative amount of activated PKD1  
432 decreases since DIV 2 and maintains at a certain level since DIV 7 in the mouse  
433 hippocampal cultures (Czondor et al., 2009). To examine whether the effects of PKD1  
434 on spine development rely on its kinase activity or not, a kinase-dead version of  
435 hPKD1 (dominant-negative hPKD1, DN-hPKD1) was overexpressed and it decreased  
436 the spine density, spine area and mEPSC frequency compared to the empty vector  
437 (Fig. 2A, B), suggesting that the kinase activity is indispensable for synapse formation

---

438 and function.

439 To investigate whether endogenous PKD1 is required for spine development, we  
440 constructed a short hairpin RNA of rat PKD1 (hereafter referred to as shPKD1) and  
441 examined its silencing efficiency by Western blot. The expression of myc-tagged rat  
442 PKD1 (rat-hPKD1) was significantly decreased in shPKD1-transfected N2a cells  
443 compared to that of control shRNA (shGFP)-transfected cells. Besides, shPKD1 had  
444 no effect on hPKD1, and hPKD1 rescued the knockdown effects of shPKD1,  
445 excluding off-target effects of the shRNA (Fig. 2C). Knockdown of PKD1  
446 significantly decreased the spine density, spine area and mEPSC frequency in cultured  
447 neurons, and these could be rescued by overexpression of hPKD1. However,  
448 DN-hPKD1 failed to rescue the spine phenotypes and synaptic transmission defects  
449 caused by PKD1 knockdown (Fig. 2D,E; for spine density,  $p < 0.0001$ ,  $F_{(3,62)} = 31.52$ ,  
450 one-way ANOVA; for spine area,  $p < 0.0001$ ,  $F_{(3,57)} = 51.76$ , one-way ANOVA; for  
451 mEPSC frequency,  $p < 0.0001$ ,  $F_{(3,31)} = 14.88$ , one-way ANOVA; for mEPSC  
452 amplitude,  $p = 0.0307$ ,  $F_{(3,31)} = 3.374$ , one-way ANOVA). These results indicate that  
453 PKD1 is both necessary and sufficient to promote functional synapses formation in  
454 cultured hippocampal neurons.

455 Since membrane N-cadherin promotes synapse formation during development  
456 (Benson and Tanaka, 1998; Togashi et al., 2002), PKD1 might exert its effects by  
457 regulating the localization of N-cadherin on neuronal membrane. We did biotinylation  
458 assays on N-cadherin in C6 cells transfected with wild-type or dominant-negative  
459 hPKD1 to evaluate their effects on the membrane distribution of N-cadherin. The

---

460 results showed that overexpression of GFP-hPKD1 promoted the surface localization  
461 of N-cadherin, whereas GFP-DN-hPKD1 reduced the amount of N-cadherin on the  
462 cell surface (Fig. 3A;  $p = 0.0002$ ;  $F_{(2,9)} = 25.77$ ; one-way ANOVA), demonstrating  
463 that the kinase activity of PKD1 is responsible for its regulation of the cell surface  
464 localization of N-cadherin.

465 The results above suggest that PKD1 very likely functions upstream of N-cadherin. If  
466 so, the reduced spine density, spine area and synaptic strength caused by PKD1  
467 knockdown should be rescued by overexpression of N-cadherin. Indeed,  
468 morphological and electrophysiological studies showed that overexpression of  
469 N-cadherin rescued the phenotypes caused by knocking down PKD1, whereas  
470 overexpression of PKD1 failed to rescue the knockdown effect of N-cadherin (Fig. 3B,  
471 C; for spine density,  $p < 0.0001$ ,  $F_{(4,82)} = 21.29$ , one-way ANOVA; for spine area,  $p <$   
472  $0.0001$ ,  $F_{(4,67)} = 93.26$ , one-way ANOVA; for mEPSC frequency,  $p < 0.0001$ ,  $F_{(4,50)} =$   
473  $14.72$ , one-way ANOVA; for mEPSC amplitude,  $p = 0.0915$ ,  $F_{(4,51)} = 2.122$ , one-way  
474 ANOVA). Taken together, these results show that PKD1 regulates the membrane  
475 localization of N-cadherin to promote synapse formation and function.

476

477 **PKD1 binds directly to the C-terminus of N-cadherin at amino acid residues**  
478 **836-871**

479 The results described above demonstrate that PKD1 interacts with N-cadherin *in vitro*  
480 and in cultured hippocampal neurons (Fig. 1A, C). To identify the critical amino acids  
481 in N-cadherin that are responsible for its binding with PKD1, we generated a series of

---

482 GST-tagged constructs expressing various portions of the C-terminus of N-cadherin  
483 (N-cad-C-ter) and tested them with His-PKD1. We found that the fragment of  
484 836-871 amino acids had the highest affinity for binding with PKD1 (Fig. 4A, lane 5  
485 compared to lane 4 and 6), suggesting that amino acid residues 836-871 of N-cadherin  
486 are necessary and sufficient for its binding with PKD1.

487 We further explored the function of PKD1 binding with N-cadherin through an analog  
488 of N-cadherin with a deletion of the PKD1 binding motif (N-cad $\Delta$ 836-871). The  
489 results of surface biotinylation assays showed that a much lower proportion of  
490 N-cad $\Delta$ 836-871 was present on the cell membrane compared to full-length  
491 N-cadherin (Fig. 4B;  $p = 0.0022$ ,  $t_{(2)} = 21.40$ , paired  $t$ -test). Overexpression of  
492 full-length N-cadherin increased the spine density, spine area and mEPSC frequency,  
493 whereas overexpression of N-cad $\Delta$ 836-871 caused a reduction in these parameters  
494 (Fig. 4C,D; for spine density,  $p < 0.0001$ ,  $F_{(2,45)} = 38.83$ , one-way ANOVA; for spine  
495 area,  $p < 0.0001$ ,  $F_{(2,41)} = 56.16$ , one-way ANOVA; for mEPSC frequency,  $p < 0.0001$ ,  
496  $F_{(2,48)} = 36.78$ , one-way ANOVA; for mEPSC amplitude,  $p = 0.0808$ ,  $F_{(2,48)} = 2.653$ ,  
497 one-way ANOVA). Furthermore, N-cad $\Delta$ 836-871 failed to rescue the reduced mEPSC  
498 frequency caused by PKD1 knockdown (Fig. 4E; for mEPSC frequency,  $p = 0.0003$ ,  
499  $F_{(3,49)} = 7.695$ , one-way ANOVA; for mEPSC amplitude,  $p = 0.0461$ ,  $F_{(3,49)} = 2.865$ ,  
500 one-way ANOVA). These results suggest that deletion of amino acids 836-871 of  
501 N-cadherin blocks the effects of PKD1 on synapse formation and function.

502 To disrupt the binding of endogenous PKD1 and N-cadherin, we created an  
503 interfering peptide of which the sequence corresponds to amino acids 836-871 of

---

504 N-cadherin, and made it cell-permeable by fusing it to the HIV TAT protein  
505 (RKKRRQRRR) (Brooks et al., 2005; Wang et al., 2014). This peptide is referred to  
506 as TAT-836-871. A peptide corresponding to a randomly scrambled version of  
507 residues 836-871 of N-cadherin fused to the TAT protein was used as a control  
508 (TAT-scramble). TAT-836-871 efficiently disrupted the binding of PKD1 and  
509 N-cadherin in cultured neurons (Fig. 6A;  $p = 0.0006$ ,  $t_{(5)} = 7.602$ , paired  $t$ -test). It also  
510 led to a significant reduction in the surface localization of N-cadherin (Fig. 6B;  $p =$   
511  $0.0075$ ,  $t_{(2)} = 11.44$ , paired  $t$ -test). Moreover, TAT-836-871 treatment of cultured  
512 neurons caused a reduction in the spine density and spine area, as well as an inhibition  
513 of synaptic transmission, compared to treatment with TAT-scramble (Fig. 6C,D; for  
514 spine density,  $p = 0.0016$ ,  $t_{(23)} = 3.576$ , unpaired  $t$ -test; for spine area,  $p < 0.0001$ ,  $t_{(24)}$   
515  $= 6.243$ , unpaired  $t$ -test; for mEPSC frequency,  $p = 0.0077$ ,  $t_{(18)} = 3.002$ , unpaired  
516  $t$ -test; for mEPSC amplitude,  $p = 0.3826$ ,  $t_{(18)} = 0.8949$ , unpaired  $t$ -test). These results  
517 confirm that the direct binding of PKD1 to amino acid residues 836-871 of  
518 N-cadherin is critical for functional synapse formation.

519

#### 520 **N-cadherin is a novel substrate of PKD1**

521 PKD1 participates in a variety of cellular processes through its phosphorylation of  
522 downstream substrates (Cabrera-Poch et al., 2004; Doppler et al., 2005; Krueger et al.,  
523 2010; Rozengurt, 2011). Based on our discoveries that PKD1 phosphorylates  
524 N-cadherin (Fig. 1B) and that the kinase activity of PKD1 is essential for functional  
525 synapse formation and the membrane distribution of N-cadherin (Figs. 2, 3), we

---

526 sought to identify the critical sites at which PKD1 phosphorylates N-cadherin and  
527 explore the subsequent effects of the phosphorylation.

528 First we generated a series of His-tagged constructs encoding successively longer  
529 fragments of N-cad-C-ter; each longer construct encodes several additional serines or  
530 threonines that might possibly be phosphorylated (Fig. 5A). Phosphorylation assays  
531 showed that PKD1 phosphorylated His-747-872 (Fig. 5B), which contains Ser 869,  
532 871, 872. Because these three serines have leucines in their -5 positions which match  
533 the consensus phosphorylation sequence of PKD1 (Nishikawa et al., 1998), we  
534 speculated that Ser 869, 871, 872 in N-cadherin might be PKD1 phosphorylation sites.  
535 The mutation of these three serine residues to alanines decreased the phosphorylation  
536 of N-cadherin by PKD1 (Fig. 5C). These results suggest that N-cadherin is a novel  
537 substrate of PKD1 in the nervous system and can be phosphorylated at Ser 869, 871,  
538 872.

539 We next mutated the three serines to alanines to generate an analog of N-cadherin  
540 (N-cad mut) for further study. Biotinylation assays showed that much less N-cad mut  
541 was distributed on the membrane compared to wild type N-cadherin (Fig. 5D;  $p =$   
542  $0.0026$ ,  $t_{(3)} = 9.283$ , paired  $t$ -test). Overexpression of N-cadherin increased the spine  
543 density, spine area and mEPSC frequency, whereas N-cad mut lost the ability to  
544 promote synapse formation or function (Fig. 5F, G; for spine density,  $p < 0.0001$ ,  
545  $F_{(2,46)} = 46.09$ , one-way ANOVA; for spine area,  $p < 0.0001$ ,  $F_{(2,40)} = 28.12$ , one-way  
546 ANOVA; for mEPSC frequency,  $p < 0.0001$ ,  $F_{(2,45)} = 46.86$ , one-way ANOVA; for  
547 mEPSC amplitude,  $p = 0.0968$ ,  $F_{(2,45)} = 2.461$ , one-way ANOVA). Like

---

548 N-cad $\Delta$ 836-871, N-cad mut also failed to rescue the reduced mEPSC frequency  
549 caused by PKD1 knockdown (Fig. 5H; for mEPSC frequency,  $p < 0.0001$ ,  $F_{(3,55)} =$   
550 15.09, one-way ANOVA; for mEPSC amplitude,  $p = 0.1346$ ,  $F_{(3,55)} = 1.935$ , one-way  
551 ANOVA). These results suggest that phosphorylation of N-cadherin by PKD1 is  
552 necessary for functional synapse formation.

553 To further investigate the roles of N-cadherin phosphorylation by endogenous PKD1,  
554 we created an interfering peptide, TAT-N-cad S3, containing the three identified serine  
555 phosphorylation sites, to compete with endogenous N-cadherin for the  
556 phosphorylation by PKD1. TAT-N-cad S3A, in which the three serines were mutated  
557 to alanines, was used as a control. TAT-N-cad S3 reduced the amount of N-cadherin  
558 on cell surface as expected (Fig. 6F;  $p = 0.0066$ ,  $t_{(2)} = 12.25$ , paired  $t$ -test). Likewise,  
559 TAT-N-cad S3 led to a significant reduction in the spine density, spine area, mEPSC  
560 frequency and amplitude (Fig. 6G, H; for spine density,  $p = 0.0017$ ,  $t_{(32)} = 3.425$ ,  
561 unpaired  $t$ -test; for spine area,  $p < 0.0001$ ,  $t_{(32)} = 4.837$ , unpaired  $t$ -test; for mEPSC  
562 frequency,  $p < 0.0001$ ,  $t_{(27)} = 9.636$ , unpaired  $t$ -test; for mEPSC amplitude,  $p = 0.0172$ ,  
563  $t_{(27)} = 2.538$ , unpaired  $t$ -test). Additionally, we found that interference with PKD1  
564 phosphorylating N-cadherin also affected the physical association between them (Figs.  
565 5E, 6E; in Fig. 5E,  $p = 0.0365$ ,  $t_{(4)} = 3.093$ , unpaired  $t$ -test; in Fig. 6E,  $p = 0.0120$ ,  $t_{(3)}$   
566  $= 5.472$ , paired  $t$ -test).

567 Thus far, we have demonstrated that N-cadherin is a novel substrate of PKD1 and  
568 have shown that PKD1 phosphorylates N-cadherin at Ser 869, 871, 872, which are  
569 essential for the effects of PKD1 on synapse formation and function.

570

---

571 **Interaction of PKD1 and N-cadherin promotes the binding of N-cadherin to**  
572  **$\beta$ -catenin**

573 It has been reported that the C-terminal domain of N-cadherin interacts with  $\beta$ -catenin,  
574 which interacts with  $\alpha$ -catenin and F-actin to stabilize the membrane localization of  
575 N-cadherin (Arikkath and Reichardt, 2008). This prompted the idea that the increased  
576 cell surface abundance of N-cadherin regulated by PKD1 might be due to enhanced  
577 binding of N-cadherin to  $\beta$ -catenin. Overexpression of hPKD1 increased the binding  
578 of N-cadherin to  $\beta$ -catenin, whereas overexpression of DN-hPKD1 curtailed their  
579 interaction (Fig. 7A;  $p < 0.0001$ ,  $F_{(2,12)} = 35.64$ , one-way ANOVA), suggesting that  
580 the kinase activity of PKD1 is critical for the binding of N-cadherin to  $\beta$ -catenin.  
581 Furthermore, overexpression of N-cad $\Delta$ 836-871 or N-cad mut decreased the binding  
582 of N-cadherin to  $\beta$ -catenin compared to wild-type N-cadherin (Fig. 7B, C; in Fig. 7B,  
583  $p = 0.0181$ ,  $t_{(4)} = 3.865$ , unpaired  $t$ -test; in Fig. 7C,  $p = 0.0017$ ,  $t_{(3)} = 10.90$ , paired  
584  $t$ -test). These results provide a possible mechanism for the regulation of the  
585 membrane localization of N-cadherin by PKD1: the interactions between PKD1 and  
586 N-cadherin, including the binding and phosphorylation of N-cadherin by PKD1,  
587 promote the association between N-cadherin and  $\beta$ -catenin, leading to increased  
588 membrane localization of N-cadherin.

589

590 **PKD1 is a mediator of the activity-dependent dendritic spine development**

---

591 External environments can reshape neural circuits through the dynamic changes of  
592 synapses (Bozdagi et al., 2000; Johansson and Belichenko, 2002). Additionally, PKD1  
593 has been demonstrated to translocate to dendritic spines during synaptic development  
594 (Czondor et al., 2009). For these reasons, we postulated that PKD1 might regulate the  
595 effects of neural activity on synapse formation. KCl treatment has been widely used to  
596 mimic increased neural activity during maturation and to examine the  
597 activity-dependent effects on neuronal morphology (Sin et al., 2002; Peng et al., 2009;  
598 Qi et al., 2014). In our experiments, the extracellular  $K^+$  concentration was increased  
599 to 16 mM. Immunoprecipitation showed an activity-driven increase in the binding of  
600 PKD1 to N-cadherin (Fig. 8A;  $p = 0.0076$ ,  $t_{(6)} = 3.940$ , unpaired  $t$ -test). In agreement  
601 with previous reports that the function of N-cadherin in synapse formation is  
602 regulated by neural activity (Sugiura et al., 2009; Mendez et al., 2010), the surface  
603 localization of N-cadherin also increased after KCl stimulation (Fig. 8B;  $p = 0.0090$ ,  
604  $t_{(4)} = 4.747$ , unpaired  $t$ -test). These results reveal a neuronal activity-dependent  
605 association between PKD1 and N-cadherin, suggesting that the activity-dependent  
606 spine growth may partially rely on the PKD1-N-cadherin signaling pathway. As for  
607 the effects on neuronal morphology, increased neural activity led to significant  
608 increase in protrusion density, spine density, filopodia density (Fig. 8C<sub>2</sub>; left, group  
609 effect: KCl,  $F_{(1, 184)} = 21.64$ ,  $p < 0.0001$ , group effect: hPKD1,  $F_{(2, 184)} = 38.63$ ,  $p <$   
610  $0.0001$ ; middle, group effect: KCl,  $F_{(1, 184)} = 9.331$ ,  $p = 0.0026$ , group effect: hPKD1,  
611  $F_{(2, 184)} = 39.60$ ,  $p < 0.0001$ ; right, group effect: KCl,  $F_{(1, 184)} = 43.07$ ,  $p < 0.0001$ ,  
612 group effect: hPKD1,  $F_{(2, 184)} = 15.87$ ,  $p < 0.0001$ ), protrusion area and protrusion

---

613 length, along with mild enlargement of protrusion width (Fig. 8C<sub>3</sub>; left, group effect:  
614 KCl,  $F_{(1, 124)} = 146.2$ ,  $p < 0.0001$ , group effect: hPKD1,  $F_{(2, 124)} = 85.10$ ,  $p < 0.0001$ ;  
615 middle, group effect: KCl,  $F_{(1, 124)} = 13.21$ ,  $p = 0.0004$ , group effect: hPKD1,  $F_{(2, 124)} =$   
616  $66.31$ ,  $p < 0.0001$ ; right, group effect: KCl,  $F_{(1, 124)} = 128.7$ ,  $p < 0.0001$ , group effect:  
617 hPKD1,  $F_{(2, 124)} = 43.58$ ,  $p < 0.0001$ ), and these changes were maintained by  
618 overexpression of hPKD1 but prevented by overexpression of DN-hPKD1. We also  
619 noted that KCl stimulation didn't cause significant changes in protrusion density,  
620 spine density and filopodia density for neurons transfected with hPKD1 (Fig. 8C<sub>2</sub>),  
621 which might be due to the saturation effects of hPKD1 overexpressing leading to a  
622 limited extent of protrusion growth. These data demonstrate that the kinase activity of  
623 PKD1 is indispensable for activity-dependent spine growth in cultured neurons and  
624 that the interaction between PKD1 and N-cadherin partially regulates the spine  
625 growth induced by KCl stimulation *in vitro*.

626

627 **PKD1-N-cadherin interaction is critical for LTP induction and regulates synaptic**  
628 **plasticity**

629 To investigate the effects of interfering peptides on synaptic plasticity,  
630 electrophysiological recordings were performed in rat hippocampal slices to measure  
631 LTP after a bilateral injection of TAT-836-871, TAT-N-cad S3 or respective control  
632 peptides into the CA1 region of the hippocampus (Fig. 9A, B). Immunoprecipitation  
633 assays showed that TAT-836-871 injection did decrease PKD1 binding to N-cadherin  
634 in the hippocampus *in vivo* (Fig. 9D;  $p = 0.0299$ ,  $t_{(2)} = 5.649$ , paired *t*-test). LTP is

---

635 critically involved not only in learning and memory but also in the activity-dependent  
636 development of neural circuits and synaptic plasticity (Bliss and Collingridge, 1993;  
637 Engert and Bonhoeffer, 1999). We obtained hippocampal slices 12 h after peptide  
638 injection and induced LTP in Schaffer collaterals using high-frequency stimulation  
639 (HFS) (Fig. 9C). In slices from rats injected with interfering peptides, the initial  
640 strength of LTP was decreased and the field EPSP (fEPSP) slope diminished to  
641 baseline by ~30 min after induction, whereas in slices from control animals  
642 significant and robust LTP was maintained for the entire recording period (Fig. 9E, F).  
643 The paired-pulse ratio (PPR) is primarily associated with changes in presynaptic  
644 transmitter release (Hessler et al., 1993). We measured the PPR after peptide injection  
645 and calculated it at every inter-stimulation interval (ISI) (50–300 ms) (Fig. 9G, H; in  
646 Fig. 9G,  $p = 0.0498$ ,  $t_{(23)} = 2.071$ , unpaired  $t$ -test; in Fig. 9H,  $p = 0.0481$ ,  $t_{(30)} = 2.061$ ,  
647 unpaired  $t$ -test). The increased PPR observed in the slices injected with the interfering  
648 peptides indicated a reduced probability of transmitter release, although no significant  
649 differences at each ISI time point between groups were detected. These results  
650 demonstrate that synaptic plasticity is directly modulated by the interaction of PKD1  
651 and N-cadherin and that their interaction may have potential effects on learning and  
652 memory.

653

#### 654 **Discussion**

655 The results of this study indicate a direct functional interaction between PKD1 and  
656 N-cadherin and identify N-cadherin as a novel substrate of PKD1 in the nervous

---

657 system. Our work demonstrates that the interaction between PKD1 and N-cadherin  
658 increases the surface localization of N-cadherin, leading to increases in spine density,  
659 spine area and transmission efficacy that are correlated with synaptic potentiation (Fig.  
660 10). These activity-dependent PKD1-N-cadherin interactions provide new molecular  
661 mechanisms for synapse formation and function.

662 Kinase activity and possible substrates are often first taken into account when  
663 exploring how a protein kinase works. Previous study showed that PKD1  
664 phosphorylates E-cadherin, but it remains unknown which amino acid residues in  
665 cadherins are phosphorylated by PKD1 (Jaggi et al., 2005). In this study, we identified  
666 the sites in N-cadherin phosphorylated by PKD1 as Ser 869, 871, 872. Further  
667 functional studies revealed that the three phosphorylation sites are crucial for the  
668 membrane localization of N-cadherin and synapse development, indicating that PKD1  
669 promotes synapse formation and function not only through its physical binding to  
670 N-cadherin but also by phosphorylation of N-cadherin. It is of interest that two of the  
671 observed phosphorylation sites, Ser 869 and Ser 871, are located within the PKD1  
672 binding motif (amino acids 836-871) of N-cadherin. This overlap may underlie the  
673 decreased binding of PKD1 to N-cadherin that occurs when the phosphorylation of  
674 N-cadherin by PKD1 is disrupted (Figs. 5E, 6E). We also found that increasing  
675 neuronal activity promoted the binding of PKD1 and N-cadherin, and the surface  
676 localization of N-cadherin (Fig. 8A, B). From the morphological studies, KCl  
677 treatment failed to promote spine formation in DN-hPKD1 expressing neurons (Fig.  
678 8C). Combined with these results, we speculated that neuronal activity induced

---

679 surface localization of N-cadherin is dependent on PKD1 kinase activity.

680 Subcellular fractionation assay of hippocampal CA1 region of postnatal 3~4 week old

681 rats showed that PKD1 was significantly enriched in the PSD fraction (Fig. 1C),

682 which suggested that PKD1 is mainly presented in the postsynaptic compartment. Our

683 results clearly demonstrated the localization of PKD1 in adolescent rat CA1 region

684 during the late phase of neural development. Consequently, PKD1 interacts with

685 N-cadherin postsynaptically in dendritic spines. In the electrophysiological studies,

686 we observed a significant increase in mEPSC frequency but not in mEPSC amplitude

687 after overexpression of PKD1 (Fig. 2B) or N-cadherin (Figs. 4D, 5G). Alterations in

688 mEPSC frequency generally reflect changes in the number of synapses and the

689 probability of presynaptic neurotransmitter release. Combined with the subcellular

690 fractionation assay that PKD1 was presented in postsynaptic compartment, the

691 increase of mEPSC frequency was much more likely caused by the increase in

692 synapse number rather than the presynaptic changes. However, we cannot rule out the

693 possibility that these manipulations might also change the presynaptic

694 neurotransmitter release probability at existing synapses. Previous studies have

695 demonstrated that N-cadherin trans-synaptically regulates presynaptic function in a

696 retrograde manner and that knockdown of N-cadherin results in impairment of vesicle

697 exocytosis and replenishment of the readily releasable vesicle pool (Bamji et al., 2003;

698 Saglietti et al., 2007). We also observed increased PPR after disrupting

699 PKD1-N-cadherin interaction in CA1 regions (Fig. 9G, H), which suggested that this

700 impaired transmitter release was regulated by postsynaptic manipulations on

---

701 PKD1-N-cadherin interactions. Therefore, postsynaptic manipulation of PKD1 may  
702 also regulate presynaptic vesicle release through retrograde control of presynaptic  
703 N-cadherin.

704 PKD has been implicated in salt taste-induced learning in *Caenorhabditis elegans* (Fu  
705 et al., 2009) and in cocaine-induced locomotor hyperactivity (Wang et al., 2014) . A  
706 study has reported that actin stabilization needed for the enlargement of dendritic  
707 spines is dependent on PKD activity, thus impaired PKD functions attenuate LTP  
708 formation and spatial memory formation (Bencsik et al., 2015). The authors  
709 performed the Morris water maze using the kdPKD-EGFP-expressing mice during the  
710 9-10th weeks of DOX treatment. In our experiments, we specifically conducted the  
711 electrophysiological studies on adolescent animals at the age of postnatal 3-4 weeks,  
712 which corresponds to the late phase of neuronal development. We observed that  
713 disrupting PKD1-N-cadherin interaction in rat hippocampus 12 h before obtaining the  
714 acute brain slices inhibited LTP induction and maintenance (Fig. 9E, F), confirming  
715 the correlated changes in spine morphology and in synaptic plasticity *in vitro*.

716 Overall, our study demonstrates one of the multi-regulatory mechanisms of PKD1 in  
717 the late phase of neuronal development: the precise regulation of membrane  
718 N-cadherin by PKD1 is critical for synapse formation and synaptic plasticity as shown  
719 in our working hypothesis (Fig. 10). Our study also provides a possible therapeutic  
720 target for the clinical treatment of neurodevelopmental diseases such as schizophrenia  
721 and neurodegenerative diseases such as Alzheimer's disease.

722

---

723 **References**

- 724 Arikath J, Reichardt LF (2008) Cadherins and catenins at synapses: roles in  
725 synaptogenesis and synaptic plasticity. *Trends Neurosci* 31:487-494.
- 726 Avriyanti E, Atik N, Kunii M, Furumoto N, Iwano T, Yoshimura S, Harada R, Harada  
727 A (2015) Functional redundancy of protein kinase D1 and protein kinase D2 in  
728 neuronal polarity. *Neurosci Res* 95:12-20.
- 729 Bacchelli E, Ceroni F, Pinto D, Lomartire S, Giannandrea M, D'Adamo P, Bonora E,  
730 Parchi P, Tancredi R, Battaglia A, Maestrini E (2014) A CTNNA3 compound  
731 heterozygous deletion implicates a role for alphaT-catenin in susceptibility to  
732 autism spectrum disorder. *J Neurodev Disord* 6:17.
- 733 Bamji SX, Shimazu K, Kimes N, Huelsken J, Birchmeier W, Lu B, Reichardt LF  
734 (2003) Role of beta-catenin in synaptic vesicle localization and presynaptic  
735 assembly. *Neuron* 40:719-731.
- 736 Bencsik N, Sziber Z, Liliom H, Tarnok K, Borbely S, Gulyas M, Ratkai A, Szucs A,  
737 Hazai-Novak D, Ellwanger K, Racz B, Pfizenmaier K, Hausser A, Schlett K  
738 (2015) Protein kinase D promotes plasticity-induced F-actin stabilization in  
739 dendritic spines and regulates memory formation. *The Journal of cell biology*  
740 210:771-783.
- 741 Benson DL, Tanaka H (1998) N-cadherin redistribution during synaptogenesis in  
742 hippocampal neurons. *J Neurosci* 18:6892-6904.
- 743 Bisbal M, Conde C, Donoso M, Bollati F, Sesma J, Quiroga S, Diaz Anel A, Malhotra  
744 V, Marzolo MP, Caceres A (2008) Protein kinase d regulates trafficking of

- 
- 745 dendritic membrane proteins in developing neurons. *The Journal of*  
746 *neuroscience* : the official journal of the Society for Neuroscience  
747 28:9297-9308.
- 748 Bliss TV, Collingridge GL (1993) A synaptic model of memory: long-term  
749 potentiation in the hippocampus. *Nature* 361:31-39.
- 750 Bozdagi O, Shan W, Tanaka H, Benson DL, Huntley GW (2000) Increasing numbers  
751 of synaptic puncta during late-phase LTP: N-cadherin is synthesized, recruited  
752 to synaptic sites, and required for potentiation. *Neuron* 28:245-259.
- 753 Brooks H, Lebleu B, Vives E (2005) Tat peptide-mediated cellular delivery: back to  
754 basics. *Adv Drug Deliv Rev* 57:559-577.
- 755 Cabrera-Poch N, Sanchez-Ruiloba L, Rodriguez-Martinez M, Iglesias T (2004) Lipid  
756 raft disruption triggers protein kinase C and Src-dependent protein kinase D  
757 activation and Kidins220 phosphorylation in neuronal cells. *The Journal of*  
758 *biological chemistry* 279:28592-28602.
- 759 Carlin RK, Grab DJ, Cohen RS, Siekevitz P (1980) Isolation and characterization of  
760 postsynaptic densities from various brain regions: enrichment of different  
761 types of postsynaptic densities. *The Journal of cell biology* 86:831-845.
- 762 Cho KO, Hunt CA, Kennedy MB (1992) The rat brain postsynaptic density fraction  
763 contains a homolog of the *Drosophila* discs-large tumor suppressor protein.  
764 *Neuron* 9:929-942.
- 765 Czondor K, Ellwanger K, Fuchs YF, Lutz S, Gulyas M, Mansuy IM, Hausser A,  
766 Pfizenmaier K, Schlett K (2009) Protein kinase D controls the integrity of

- 
- 767 Golgi apparatus and the maintenance of dendritic arborization in hippocampal  
768 neurons. *Molecular biology of the cell* 20:2108-2120.
- 769 Doppler H, Storz P, Li J, Comb MJ, Toker A (2005) A phosphorylation state-specific  
770 antibody recognizes Hsp27, a novel substrate of protein kinase D. *J Biol Chem*  
771 280:15013-15019.
- 772 Engert F, Bonhoeffer T (1999) Dendritic spine changes associated with hippocampal  
773 long-term synaptic plasticity. *Nature* 399:66-70.
- 774 Friedman LG, Benson DL, Huntley GW (2015) Cadherin-based transsynaptic  
775 networks in establishing and modifying neural connectivity. *Curr Top Dev*  
776 *Biol* 112:415-465.
- 777 Fu Y, Ren M, Feng H, Chen L, Altun ZF, Rubin CS (2009) Neuronal and intestinal  
778 protein kinase d isoforms mediate Na<sup>+</sup> (salt taste)-induced learning. *Science*  
779 *signaling* 2:ra42.
- 780 Gumbiner BM (2005) Regulation of cadherin-mediated adhesion in morphogenesis.  
781 *Nat Rev Mol Cell Biol* 6:622-634.
- 782 Hessler NA, Shirke AM, Malinow R (1993) The probability of transmitter release at a  
783 mammalian central synapse. *Nature* 366:569-572.
- 784 Iglesias T, Rozengurt E (1998) Protein kinase D activation by mutations within its  
785 pleckstrin homology domain. *J Biol Chem* 273:410-416.
- 786 Iglesias T, Waldron RT, Rozengurt E (1998) Identification of in vivo phosphorylation  
787 sites required for protein kinase D activation. *J Biol Chem* 273:27662-27667.
- 788 Jaggi M, Rao PS, Smith DJ, Wheelock MJ, Johnson KR, Hemstreet GP, Balaji KC

- 
- 789 (2005) E-cadherin phosphorylation by protein kinase D1/protein kinase C{mu}  
790 is associated with altered cellular aggregation and motility in prostate cancer.  
791 Cancer Res 65:483-492.
- 792 Johannes FJ, Prestle J, Eis S, Oberhagemann P, Pfizenmaier K (1994) PKC $\alpha$  is a novel,  
793 atypical member of the protein kinase C family. J Biol Chem 269:6140-6148.
- 794 Johansson BB, Belichenko PV (2002) Neuronal plasticity and dendritic spines: effect  
795 of environmental enrichment on intact and postischemic rat brain. J Cereb  
796 Blood Flow Metab 22:89-96.
- 797 Kandel ER, Dudai Y, Mayford MR (2014) The molecular and systems biology of  
798 memory. Cell 157:163-186.
- 799 Krueger DD, Osterweil EK, Bear MF (2010) Activation of mGluR5 induces rapid and  
800 long-lasting protein kinase D phosphorylation in hippocampal neurons.  
801 Journal of molecular neuroscience : MN 42:1-8.
- 802 Lewallen KA, Shen YA, De la Torre AR, Ng BK, Meijer D, Chan JR (2011) Assessing  
803 the role of the cadherin/catenin complex at the Schwann cell-axon interface  
804 and in the initiation of myelination. J Neurosci 31:3032-3043.
- 805 Mendez P, De Roo M, Poglia L, Klausner P, Muller D (2010) N-cadherin mediates  
806 plasticity-induced long-term spine stabilization. J Cell Biol 189:589-600.
- 807 Nishikawa K, Toker A, Wong K, Marignani PA, Johannes FJ, Cantley LC (1998)  
808 Association of protein kinase C $\mu$  with type II phosphatidylinositol 4-kinase  
809 and type I phosphatidylinositol-4-phosphate 5-kinase. J Biol Chem  
810 273:23126-23133.

- 
- 811 Peng YR, He S, Marie H, Zeng SY, Ma J, Tan ZJ, Lee SY, Malenka RC, Yu X (2009)  
812 Coordinated changes in dendritic arborization and synaptic strength during  
813 neural circuit development. *Neuron* 61:71-84.
- 814 Qi C, Liu S, Qin R, Zhang Y, Wang G, Shang Y, Wang Y, Liang J (2014) Coordinated  
815 regulation of dendrite arborization by epigenetic factors CDYL and EZH2.  
816 *The Journal of neuroscience : the official journal of the Society for*  
817 *Neuroscience* 34:4494-4508.
- 818 Rozengurt E (2011) Protein kinase D signaling: multiple biological functions in health  
819 and disease. *Physiology (Bethesda)* 26:23-33.
- 820 Saglietti L, Dequidt C, Kamieniarz K, Rousset MC, Valnegri P, Thoumine O, Beretta  
821 F, Fagni L, Choquet D, Sala C, Sheng M, Passafaro M (2007) Extracellular  
822 interactions between GluR2 and N-cadherin in spine regulation. *Neuron*  
823 54:461-477.
- 824 Schrick C, Fischer A, Srivastava DP, Tronson NC, Penzes P, Radulovic J (2007)  
825 N-cadherin regulates cytoskeletally associated IQGAP1/ERK signaling and  
826 memory formation. *Neuron* 55:786-798.
- 827 Seong E, Yuan L, Arikath J (2015) Cadherins and catenins in dendrite and synapse  
828 morphogenesis. *Cell Adh Migr* 9:202-213.
- 829 Sin WC, Haas K, Ruthazer ES, Cline HT (2002) Dendrite growth increased by visual  
830 activity requires NMDA receptor and Rho GTPases. *Nature* 419:475-480.
- 831 Sugiura H, Tanaka H, Yasuda S, Takemiya T, Yamagata K (2009) Transducing  
832 neuronal activity into dendritic spine morphology: new roles for p38 MAP

- 
- 833 kinase and N-cadherin. *Neuroscientist* 15:90-104.
- 834 Tahirovic S, Bradke F (2009) Neuronal polarity. *Cold Spring Harb Perspect Biol*  
835 1:a001644.
- 836 Togashi H, Abe K, Mizoguchi A, Takaoka K, Chisaka O, Takeichi M (2002) Cadherin  
837 regulates dendritic spine morphogenesis. *Neuron* 35:77-89.
- 838 Tucci V et al. (2014) Dominant beta-catenin mutations cause intellectual disability  
839 with recognizable syndromic features. *J Clin Invest* 124:1468-1482.
- 840 Uribe-Arias A, Posada-Duque RA, Gonzalez-Billault C, Villegas A, Lopera F,  
841 Cardona-Gomez GP (2016) p120-catenin is necessary for neuroprotection  
842 induced by CDK5 silencing in models of Alzheimer's disease. *J Neurochem*  
843 138:624-639.
- 844 Valverde AM, Sinnett-Smith J, Van Lint J, Rozengurt E (1994) Molecular cloning and  
845 characterization of protein kinase D: a target for diacylglycerol and phorbol  
846 esters with a distinctive catalytic domain. *Proc Natl Acad Sci U S A*  
847 91:8572-8576.
- 848 Wang N, Su P, Zhang Y, Lu J, Xing B, Kang K, Li W, Wang Y (2014) Protein kinase  
849 D1-dependent phosphorylation of dopamine D1 receptor regulates  
850 cocaine-induced behavioral responses. *Neuropsychopharmacology*  
851 39:1290-1301.
- 852 Wang Y, Kedei N, Wang M, Wang QJ, Huppler AR, Toth A, Tran R, Blumberg PM  
853 (2004) Interaction between protein kinase C $\mu$  and the vanilloid receptor type  
854 1. *J Biol Chem* 279:53674-53682.

- 
- 855 Xing BM, Yang YR, Du JX, Chen HJ, Qi C, Huang ZH, Zhang Y, Wang Y (2012)  
856 Cyclin-dependent kinase 5 controls TRPV1 membrane trafficking and the heat  
857 sensitivity of nociceptors through KIF13B. *J Neurosci* 32:14709-14721.
- 858 Yang Y, Wei M, Xiong Y, Du X, Zhu S, Yang L, Zhang C, Liu JJ (2015) Endophilin  
859 A1 regulates dendritic spine morphogenesis and stability through interaction  
860 with p140Cap. *Cell research* 25:496-516.
- 861 Yin DM, Huang YH, Zhu YB, Wang Y (2008) Both the establishment and  
862 maintenance of neuronal polarity require the activity of protein kinase D in the  
863 Golgi apparatus. *The Journal of neuroscience : the official journal of the*  
864 *Society for Neuroscience* 28:8832-8843.
- 865 Yoshimura T, Arimura N, Kaibuchi K (2006) Signaling networks in neuronal  
866 polarization. *J Neurosci* 26:10626-10630.
- 867 Zhang J, Woodhead GJ, Swaminathan SK, Noles SR, McQuinn ER, Pisarek AJ,  
868 Stocker AM, Mutch CA, Funatsu N, Chenn A (2010) Cortical neural  
869 precursors inhibit their own differentiation via N-cadherin maintenance of  
870 beta-catenin signaling. *Dev Cell* 18:472-479.
- 871
- 872

---

873 **Figure Legends**

874 **Figure 1. N-cadherin is directly associated with PKD1.**

875 **A**, IB of His-N-cad-c-ter pulldown by GST-PKD1 *in vitro*. Top, probed for  
876 His-N-cad-c-ter binding to GST-PKD1. Bottom, probed for total GST fusion protein  
877 present within each pulldown reaction. IB, immunoblot.

878 **B**, *In vitro* kinase assay showed that N-cadherin c-ter (N-cad 747-906) was  
879 phosphorylated by immunoprecipitated PKD1 (left) from the rat brain. The amount of  
880 the immunoprecipitated PKD1 was represented by the Coomassie staining IgG bands  
881 and indicated treatments were shown (right). Gö6976, a PKD1 inhibitor; Bim, a PKC  
882 inhibitor; and PMA, a PKC activator.

883 **C**, hippocampal CA1 region of rat brain lysates were fractionated by differential  
884 centrifugation and subcellular fractions were analyzed by immunoblotting with  
885 antibodies to PKD1. S1, homogenates; S2, supernatant after P2 precipitation; P2,  
886 crude synaptosomes; S3, cytosol; P3, light membranes; S4, supernatant after  
887 postsynaptic density (PSD) precipitation. SYP, synaptophysin.

888 **D**, Immunofluorescence staining for showing the co-localization of endogenous PKD1  
889 and N-cadherin in DIV15 hippocampal neurons. Arrows denote the PKD1 puncta  
890 overlapping with N-cadherin. Scale bar, 50  $\mu\text{m}$  (upper) and 5  $\mu\text{m}$  (bottom).

891

892 **Figure 2. PKD1 is essential for synapse formation and function.**

893 **A**, Representative images and quantification of spine density and area in DIV15  
894 hippocampal neurons co-transfected GFP with his-myc-tagged Vector, hPKD1, or

---

895 DN-hPKD1 at DIV8 (n = 20, 16, 16 cells, respectively, in columns shown in the  
896 graphs). Scale bars, 50  $\mu\text{m}$  (upper) and 5  $\mu\text{m}$  (bottom). \*\*\*p < 0.001 compared with  
897 Vector, ###p < 0.001 compared with hPKD1; one-way ANOVA with Bonferroni's  
898 post-hoc test.

899 **B**, Representative traces (**B<sub>1</sub>**) and plots (**B<sub>2</sub>**) of mEPSCs frequencies and amplitudes in  
900 hippocampal neurons co-transfected GFP with Vector, hPKD1 or DN-hPKD1 (n = 10,  
901 10, 11 cells, respectively). Scale bars, 10 pA and 500 ms. \*p < 0.05 and \*\*p < 0.01  
902 compared with Vector, ###p < 0.001 compared with hPKD1; one-way ANOVA with  
903 Bonferroni's post-hoc test. No significant differences in mEPSC amplitude were  
904 detected.

905 **C**, Knockdown effect of myc-tagged rat PKD1 (rat-hPKD1) by shPKD1 in N2a cells.  
906 Rat-hPKD1 is an analog of hPKD1 with the rat target sequence of shPKD1 replacing  
907 the homologous domain in hPKD1 by site-directed mutagenesis.

908 **D**, Representative images and quantification of spine density and area of DIV15  
909 hippocampal neurons transfected with shGFP+Vector, shPKD1+Vector,  
910 shPKD1+hPKD1, or shPKD1+DN-hPKD1 at DIV8 (n = 18, 17, 15, and 16 cells,  
911 respectively). Scale bar, 2.5  $\mu\text{m}$ . \*p < 0.05, \*\*p < 0.01 and \*\*\*p < 0.001 compared  
912 with shGFP+Vector, ###p < 0.001 compared with shPKD1+Vector; one-way ANOVA  
913 with Bonferroni's post-hoc test.

914 **E**, Representative traces (**E<sub>1</sub>**) and plots (**E<sub>2</sub>**) of the mEPSCs in hippocampal neurons  
915 transfected with shGFP+Vector, shPKD1+Vector, shPKD1+hPKD1, or  
916 shPKD1+DN-hPKD1 (n = 10, 11, 7, and 7 cells, respectively). Scale bars, 10 pA and

---

917 500 ms. \*\* $p < 0.01$  and \*\*\* $p < 0.001$  compared with shGFP+Vector, # $p < 0.05$   
918 compared with shPKD1+Vector; one-way ANOVA with Bonferroni's post-hoc test.  
919 No significant differences in mEPSC amplitude were detected among the groups.  
920 All graphs show the mean  $\pm$  S.E.M.

921

922 **Figure 3. PKD1 promotes synapse formation and function by acting upstream of**  
923 **N-cadherin.**

924 **A**, Surface biotinylation assay for membrane location of N-cadherin in C6 cells  
925 overexpressing GFP-Vector, GFP-hPKD1 or GFP-DN-hPKD1. Tfr, transferrin  
926 receptor.  $n = 4$ , \* $p < 0.05$  compared with GFP-Vector, ### $p < 0.001$  compared with  
927 hPKD1; one-way ANOVA with Bonferroni's post-hoc test.

928 **B**, Representative images and quantification of spine density and area of DIV15  
929 hippocampal neurons transfected with shGFP+Vector, shPKD1+Vector,  
930 shPKD1+N-cad (myc-N-cadherin), shN-cad+Vector or shN-cad+hPKD1 at DIV8 ( $n =$   
931 18, 17, 20, 16, 16 cells, respectively). Scale bar, 2.5  $\mu\text{m}$ . Same shGFP+Vector and  
932 shPKD1+Vector data as in Fig. 2D. \* $p < 0.05$  and \*\*\* $p < 0.001$  compared with  
933 shGFP+Vector, ### $p < 0.001$  compared with shPKD1+Vector; one-way ANOVA with  
934 Bonferroni's post-hoc test.

935 **C**, Representative traces (**C**<sub>1</sub>) and plots (**C**<sub>2</sub>) of mEPSC frequencies and amplitudes in  
936 hippocampal neurons transfected with shGFP+Vector, shPKD1+Vector,  
937 shPKD1+N-cad, shN-cad+Vector or shN-cad+hPKD1 ( $n = 10, 11, 8, 13, 13$  cells,  
938 respectively). Scale bars, 10 pA and 500 ms. Same shGFP+Vector and

---

939 shPKD1+Vector data as in Fig. 2E. \*\*\* $p < 0.001$  compared with shGFP+Vector, <sup>##</sup> $p <$   
940 0.01 compared with shPKD1+Vector; one-way ANOVA with Bonferroni's post-hoc  
941 test. No significant differences in mEPSC amplitude were detected.

942 All graphs show the mean  $\pm$  S.E.M

943

944 **Figure 4. PKD1 binds to N-cadherin at amino acid residues 836-871 and**  
945 **promotes functional synapse formation.**

946 **A**, Immunoblot of His-PKD1 pulldown by the indicated constructs of cytoplasmic  
947 N-cadherin. Top, probed for His-PKD1 binding to cytoplasmic N-cadherin fused to  
948 GST. Bottom, probed for total GST fusion protein present within each pulldown  
949 reaction. IB, immunoblot.

950 **B**, Membrane location of N-cadherin in N2a cells transfected with N-cad or  
951 N-cad $\Delta$ 836-871 (N-cadherin with a deletion of amino acids 836-871).  $n = 3$ , \*\* $p <$   
952 0.01; paired  $t$ -test.

953 **C**, Representative images and quantification of spine density and area of DIV15  
954 hippocampal neurons co-transfected GFP with Vector, N-cad or N-cad $\Delta$ 836-871 at  
955 DIV8 ( $n = 16, 15,$  and  $17$  cells, respectively). Scale bars,  $50 \mu\text{m}$  (upper) and  $5 \mu\text{m}$   
956 (bottom). \*\*\* $p < 0.001$  compared with Vector, <sup>###</sup> $p < 0.001$  compared with N-cad;  
957 one-way ANOVA with Bonferroni's post-hoc test.

958 **D**, Representative traces (**D<sub>1</sub>**) and plots (**D<sub>2</sub>**) of mEPSC frequencies and amplitudes in  
959 hippocampal neurons co-transfected GFP with Vector, N-cad or N-cad $\Delta$ 836-871 ( $n =$   
960  $14, 22,$  and  $15$  cells, respectively). Scale bars,  $10 \text{ pA}$  and  $500 \text{ ms}$ . \*\*\* $p < 0.001$

---

961 compared with Vector, <sup>###</sup>p < 0.001 compared with N-cad; one-way ANOVA with  
962 Bonferroni's post-hoc test.

963 **E**, Representative traces (**E<sub>1</sub>**) and plots (**E<sub>2</sub>**) of frequencies and amplitudes of the  
964 mEPSCs in hippocampal neurons transfected with shGFP+Vector, shPKD1+Vector,  
965 shPKD1+N-cad or shPKD1+N-cad $\Delta$ 836-871 (n = 10, 14, 18, and 11 cells,  
966 respectively). Scale bars, 10 pA and 500 ms. <sup>\*\*</sup>p < 0.01 compared with  
967 shGFP+Vector, <sup>#</sup>p < 0.05 and <sup>##</sup>p < 0.01 compared with shPKD1+Vector; one-way  
968 ANOVA with Bonferroni's post-hoc test. No significant differences in mEPSC  
969 amplitude were detected among the groups.

970 All graphs show the mean  $\pm$  S.E.M.

971

972 **Figure 5. PKD1 phosphorylates N-cadherin at Ser 869, 871, 872 and promotes**  
973 **functional synapse formation.**

974 **A**, Schematic depiction of cytoplasmic N-cadherin constructs illustrating the  
975 approximate localization of serine and threonine residues (black lines) that represent  
976 potential sites of phosphorylation by PKD1.

977 **B**, His-747-906 and His-747-872 containing the potential phosphorylation sites Ser  
978 869, 871, 872 were phosphorylated by PKD1.

979 **C**, N-cadherin c-ter (His-N-cad-747-906) phosphorylation by purified PKD1 was  
980 reduced by the triple mutation (His-N-cad-747-906 mut) as shown by *in vitro* kinase  
981 assay.

982 **D**, Membrane location of N-cadherin in N2a cells transfected with N-cad or

---

983 N-cad mut (N-cadherin with Ser 869, 871 and 872 mutated to alanine).  $n = 4$ ,  $**p <$   
984  $0.01$ ; paired  $t$ -test.

985 **E**, Co- immunoprecipitation of N-cadherin with PKD1 in N2a cells transfected with  
986 N-cad or N-cad mut.  $n = 3$ ,  $*p < 0.05$ ; unpaired  $t$ -test. IP, immunoprecipitation.

987 **F**, Representative images and quantification of spine density and area of DIV15  
988 hippocampal neurons co-transfected GFP with Vector, N-cad or N-cad mut at DIV8 ( $n$   
989  $= 16, 15, 18$  cells, respectively). Same Vector and N-cad data as in Fig. 4C. Scale bars,  
990  $50 \mu\text{m}$  (upper) and  $5 \mu\text{m}$  (bottom).  $**p < 0.01$  and  $***p < 0.001$  compared with  
991 Vector,  $###p < 0.001$  compared with N-cad; one-way ANOVA with Bonferroni's  
992 post-hoc test.

993 **G**, Representative mEPSC traces (**G<sub>1</sub>**) and plots (**G<sub>2</sub>**) of the frequencies and  
994 amplitudes of hippocampal neurons co-transfected GFP with Vector, N-cad or  
995 N-cad mut ( $n = 14, 22, 12$  cells, respectively). Same Vector and N-cad data as in Fig.  
996 4D. Scale bars,  $10 \text{ pA}$  and  $500 \text{ ms}$ .  $**p < 0.01$  and  $***p < 0.001$  compared with  
997 Vector,  $###p < 0.001$  compared with N-cad; one-way ANOVA with Bonferroni's  
998 post-hoc test.

999 **H**, Representative traces (**H<sub>1</sub>**) and plots (**H<sub>2</sub>**) of frequencies and amplitudes of the  
1000 mEPSCs in hippocampal neurons transfected with shGFP+Vector, shPKD1+Vector,  
1001 shPKD1+N-cad or shPKD1+N-cad mut ( $n = 10, 14, 18, \text{ and } 17$  cells, respectively).  
1002 Same shGFP+Vector, shPKD1+Vector and shPKD1+N-cad data as in Fig. 4E. Scale  
1003 bars,  $10 \text{ pA}$  and  $500 \text{ ms}$ .  $**p < 0.01$  and  $***p < 0.001$  compared with shGFP+Vector,  
1004  $##p < 0.01$  and  $###p < 0.001$  compared with shPKD1+Vector; one-way ANOVA with

---

1005 Bonferroni's post-hoc test. No significant differences in mEPSC amplitude were  
1006 detected among the groups.

1007 All graphs show the mean  $\pm$  S.E.M.

1008 **Figure 6. The effects of interfering peptides disrupting PKD1-N-cadherin**  
1009 **interactions in cultured neurons.**

1010 **A**, Effect of 3  $\mu$ M TAT-836-871 on the binding of endogenous PKD1 and N-cadherin  
1011 in cortical neurons shown by IP.  $n = 6$ , \*\*\* $p < 0.001$ ; paired  $t$ -test.

1012 **B**, Surface N-cadherin in cortical neurons treated with TAT-scramble (3  $\mu$ M) or  
1013 TAT-836-871 (3  $\mu$ M).  $n = 3$ , \* $p < 0.05$ ; paired  $t$ -test.

1014 **C**, Representative images and quantification of spine density and area in DIV15  
1015 hippocampal neurons transfected with GFP at DIV8 and treated with TAT-scramble (3  
1016  $\mu$ M) or TAT-836-871 (3  $\mu$ M) at DIV10 ( $n = 16, 17$  cells). Scale bars, 50  $\mu$ m (upper)  
1017 and 5  $\mu$ m (bottom). \*\* $p < 0.01$  and \*\*\* $p < 0.001$ ; unpaired  $t$ -test.

1018 **D**, Representative mEPSC traces (**D<sub>1</sub>**) and plots (**D<sub>2</sub>**) of the frequencies and  
1019 amplitudes of hippocampal neurons treated with TAT-scramble (3  $\mu$ M) or  
1020 TAT-836-871 (3  $\mu$ M) ( $n = 11, 9$  cells). Scale bars, 10 pA and 500 ms. \*\*\* $p < 0.01$ ;  
1021 unpaired  $t$ -test.

1022 **E**, Co-IP of PKD1 with N-cadherin from cortical neurons under TAT-N-cad S3A (3  
1023  $\mu$ M) or TAT-N-cad S3 (3  $\mu$ M) treatments.  $n = 4$ , \* $p < 0.05$ ; paired  $t$ -test.

1024 **F**, Surface N-cadherin in cortical neurons treated with TAT-N-cad S3A (3  $\mu$ M) or  
1025 TAT-N-cad S3 (3  $\mu$ M).  $n = 3$ , \*\* $p < 0.01$ ; paired  $t$ -test.

1026 **G**, Representative images and quantification of spine density and area of DIV15

---

1027 hippocampal neurons transfected with GFP at DIV8 and treated with TAT-N-cad S3A  
1028 (3  $\mu$ M) or TAT-N-cad S3 (3  $\mu$ M) at DIV10 (n = 17, 17 cells). Scale bars, 50  $\mu$ m  
1029 (upper) and 5  $\mu$ m (bottom). \*\*p < 0.01 and \*\*\*p < 0.001; unpaired *t*-test.

1030 **H**, Representative mEPSC traces (**H<sub>1</sub>**) and plots (**H<sub>2</sub>**) of the frequencies and  
1031 amplitudes of hippocampal neurons treated with TAT-N-cad S3A (3  $\mu$ M) or  
1032 TAT-N-cad S3 (3  $\mu$ M) (n = 15, 14 cells). Scale bars, 10 pA and 500 ms. \*p < 0.05 and  
1033 \*\*\*p < 0.001; unpaired *t*-test.

1034 All graphs show the mean  $\pm$  S.E.M.

1035

1036 **Figure 7. Interaction of PKD1 and N-cadherin promotes the binding of**  
1037 **N-cadherin and  $\beta$ -catenin.**

1038 **A**, Co-IP of N-cadherin with  $\beta$ -catenin in N2a cells co-transfected N-cadherin with  
1039 Vector, hPKD1 or DN-hPKD1. n = 5, \*\*p < 0.01; one-way ANOVA with Bonferroni's  
1040 post-hoc.

1041 **B&C**, N-cadherin 836-871aa deletion or Ser869, 871, 872Ala mutation decreased its  
1042 binding intensity with  $\beta$ -catenin in N2a cells. n = 3 (**B**) or 4 (**C**), \*p < 0.05 and \*\*p <  
1043 0.01; unpaired *t*-test (**B**) or paired *t*-test (**C**).

1044 All graphs show the mean  $\pm$  S.E.M.

1045

1046 **Figure 8. Neural activity promotes spine growth in a manner that depends on the**  
1047 **kinase activity of PKD1.**

1048 **A**, Activity-driven increase in N-cadherin binding to PKD1 in cultured cortical

---

1049 neurons treated with KCl (12 mM) for 12 h.  $n = 4$ ,  $**p < 0.01$ ; unpaired  $t$ -test.

1050 **B**, Activity-driven increase in the amount of membrane-associated N-cadherin in  
1051 cortical neurons treated with KCl (12 mM) for 12 h.  $n = 3$ ,  $*p < 0.05$ ; unpaired  $t$ -test.

1052 **C<sub>1</sub>**, Representative images of DIV15 hippocampal neurons transfected with GFP plus  
1053 Vector, hPKD1, or DN-hPKD1 at DIV8 and treated without or with KCl (12 mM) at  
1054 DIV10. Scale bars, 50  $\mu$  m (upper) and 5  $\mu$  m (bottom).

1055 **C<sub>2</sub>**, Quantification of protrusion density, spine density and filopodia density in  
1056 neurons from the experiment shown in **C<sub>1</sub>** ( $n = 15, 15, 15, 14, 13$ , and 18 cells,  
1057 respectively).  $***p < 0.001$ ; two-way ANOVA with Bonferroni's post-hoc test.

1058 **C<sub>3</sub>**, Quantification of protrusion area, protrusion width and protrusion length in  
1059 neurons from the experiment shown in **C<sub>1</sub>** ( $n = 15, 15, 15, 14, 13$ , and 18 cells,  
1060 respectively).  $***p < 0.001$ ; two-way ANOVA with Bonferroni's post-hoc test.

1061 All graphs show the mean  $\pm$  S.E.M.

1062

1063 **Figure 9. Disruption of the interaction of PKD1 and N-cadherin inhibits LTP and**  
1064 **increases the paired-pulse ratio in the stratum radiatum of CA1.**

1065 **A**, Column showing cannula tip placement in rats that received hippocampal injection  
1066 of interfering peptides or control peptides.

1067 **B**, Representative coronal section showing the hippocampal injection site. Scale bar,  
1068 500  $\mu$ m.

1069 **C**, Schematic of field recording configuration in CA1. The stimulating electrode was  
1070 placed in the CA3 region, and the recording electrode was placed in the stratum

---

1071 radiatum of the CA1 region to measure the field response of the Schaffer collaterals.

1072 **D**, Effect of TAT-836-871 on the binding of PKD1 to N-cadherin *in vivo* measured by

1073 IP. Hippocampal tissues obtained from rats 12 h after peptide injection respectively

1074 (10  $\mu$ g). n = 3, \*p < 0.05; paired *t*-test.

1075 **E**, Injection of TAT-836-871 (10  $\mu$ g) to CA1 region of hippocampus suppressed LTP

1076 induction (blue circles, n = 8 slices/from 7 rats) compared with the injection of

1077 TAT-scramble (gray circles, n = 9/8).

1078 **F**, Injection of TAT-N-cad S3 (10  $\mu$ g) to CA1 region of hippocampus suppressed LTP

1079 induction (red diamonds, n = 8 slices/from 7 rats) compared with TAT-N-cad S3A

1080 (gray diamonds, n = 7/7).

1081 **G&H**, Representative traces of fEPSPs evoked by paired pulses at six inter-stimulus

1082 intervals (ISI; 50 ms, 100 ms, 150 ms, 200 ms, 250 ms and 300 ms). The paired-pulse

1083 ratio in the hippocampal CA1 region was increased by TAT-836-871 (10  $\mu$ g) and

1084 TAT-N-cad S3 (10  $\mu$ g) injections compared with the injections of their control

1085 peptides respectively. \*p < 0.05; unpaired *t*-test.

1086 All graphs show the mean  $\pm$  S.E.M.

1087

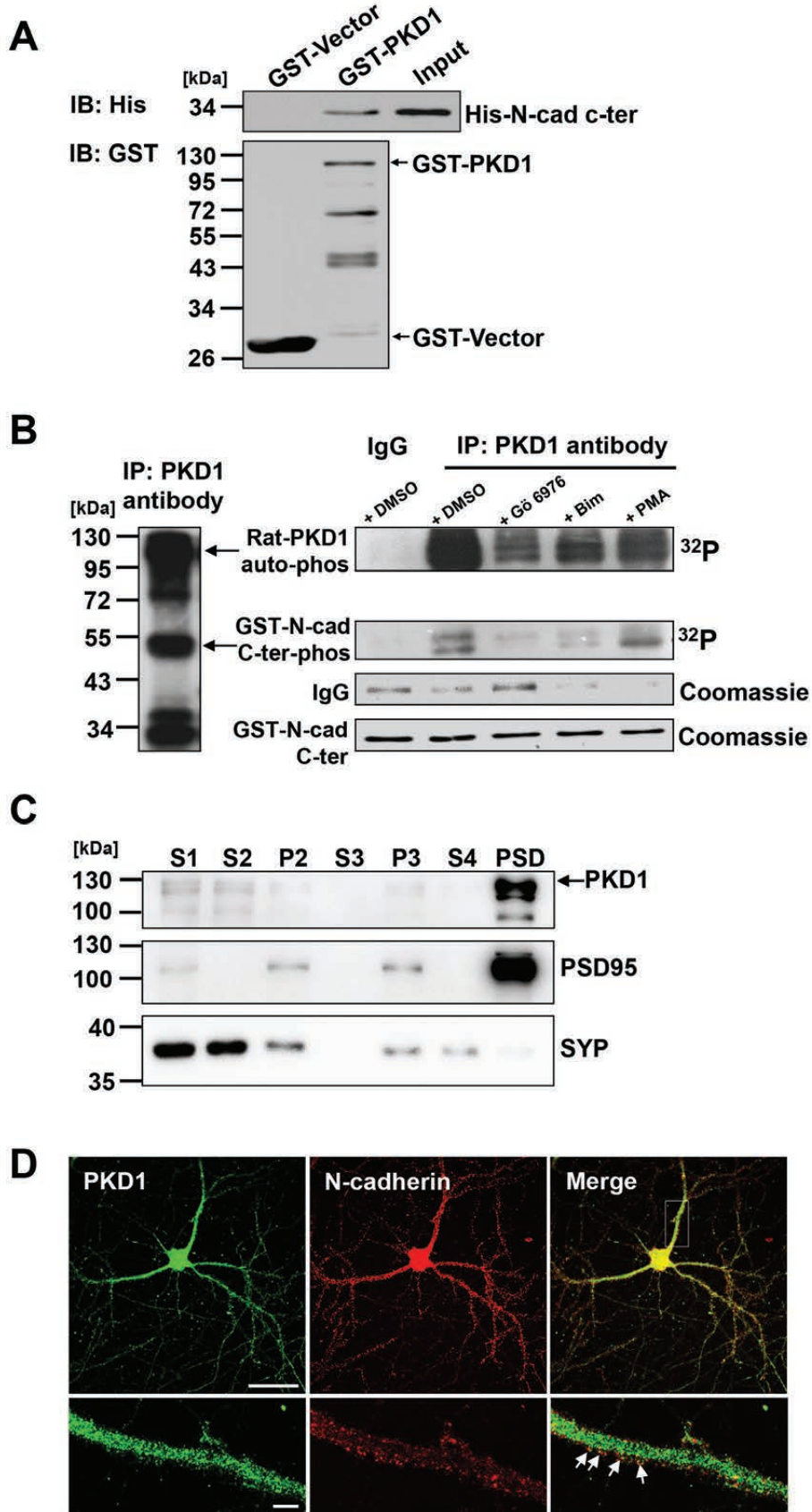
1088 **Figure 10. Working Model.** PKD1 binds to N-cadherin at amino acid residues

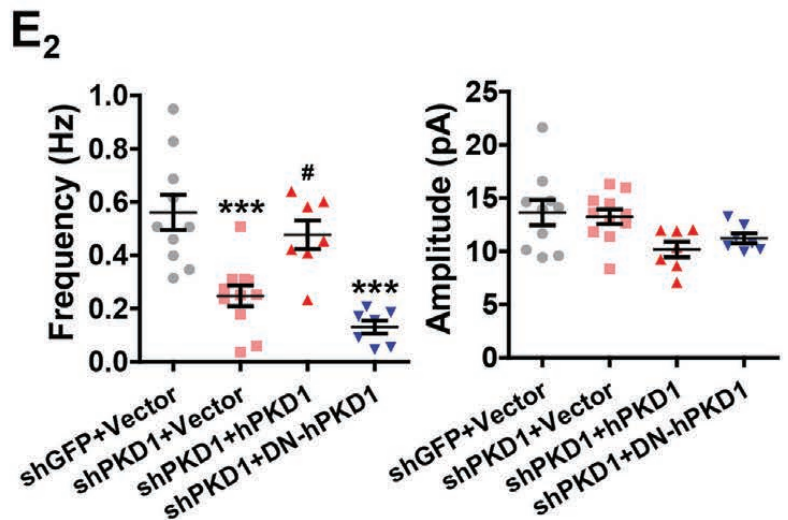
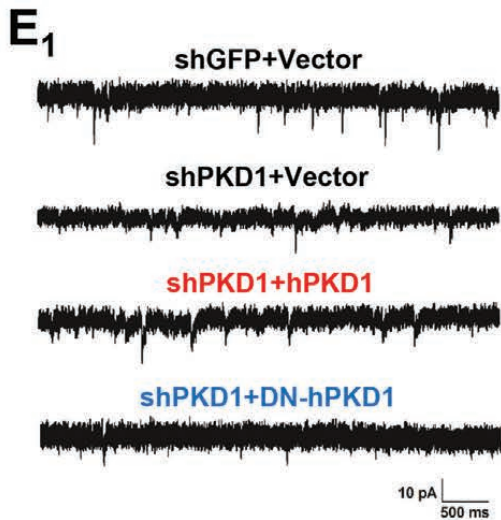
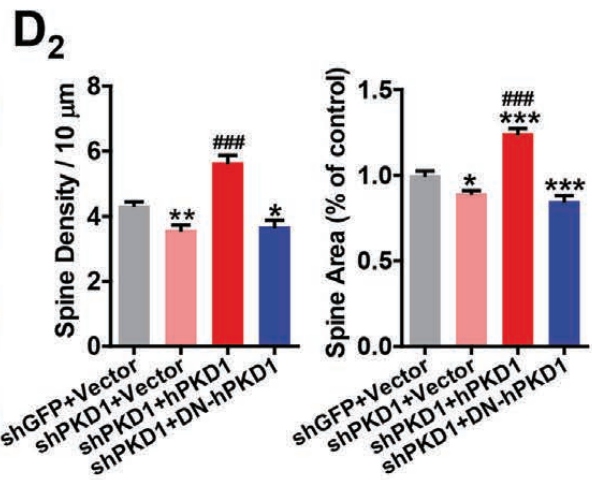
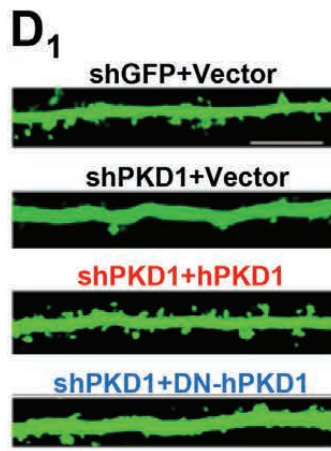
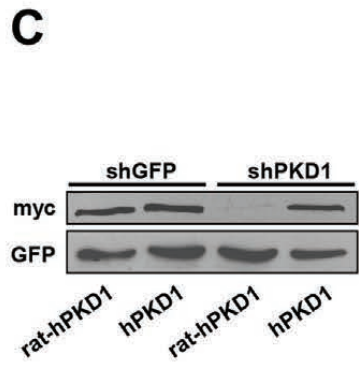
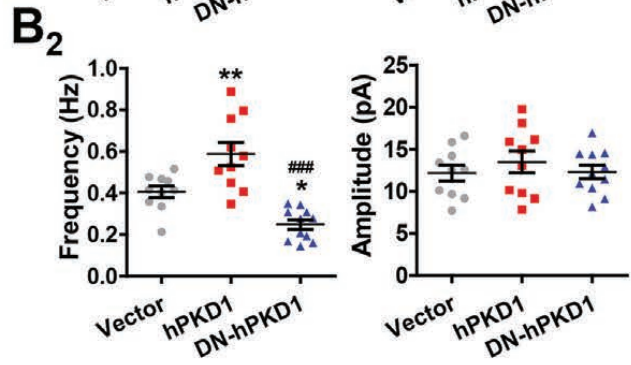
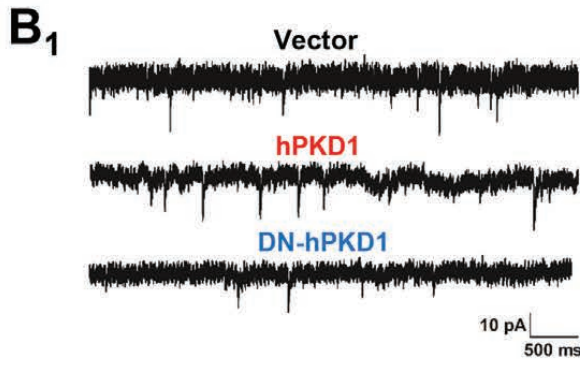
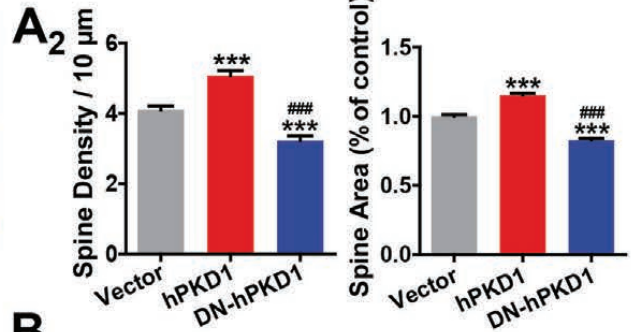
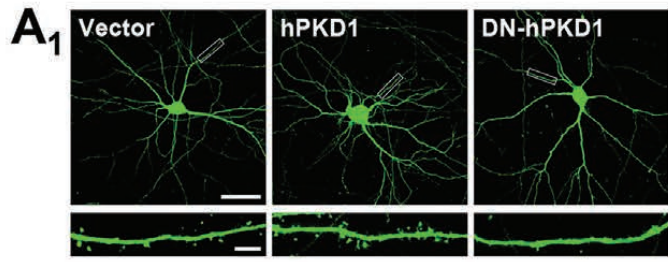
1089 836-871 and phosphorylates it at Ser 869, 871 and 872. Disruption of the modification

1090 of N-cadherin by PKD1 impairs the binding of N-cadherin to  $\beta$ -catenin and the

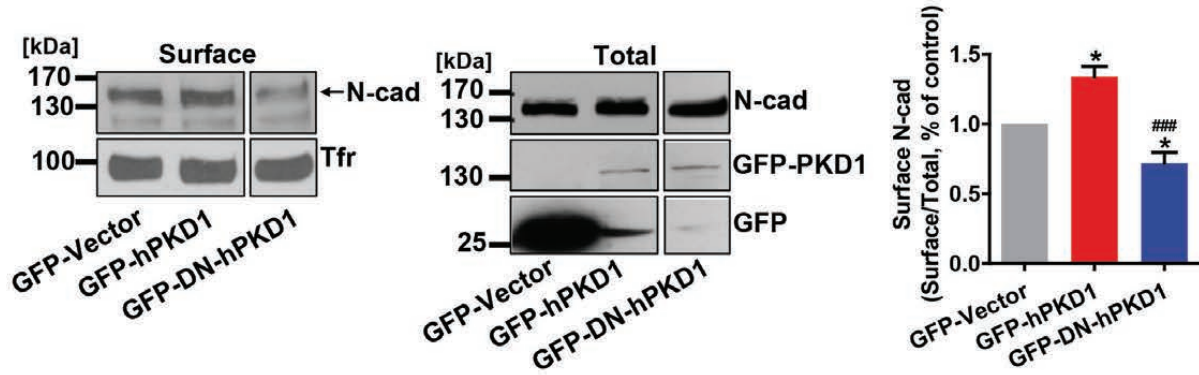
1091 membrane localization of N-cadherin, thereby inhibiting synapse formation and

1092 synaptic plasticity.

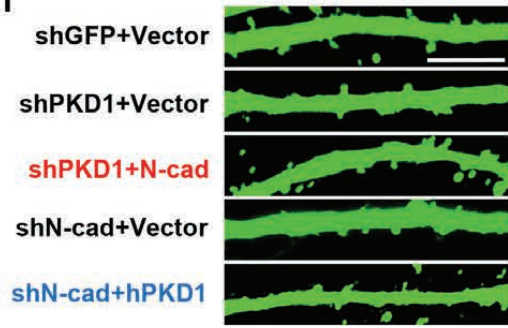




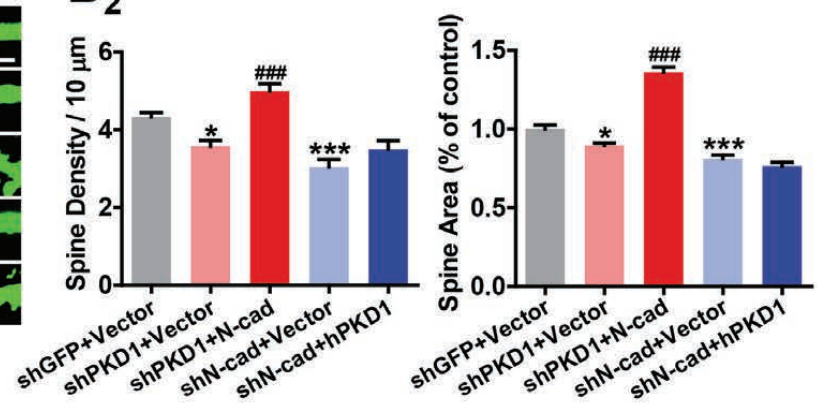
**A**



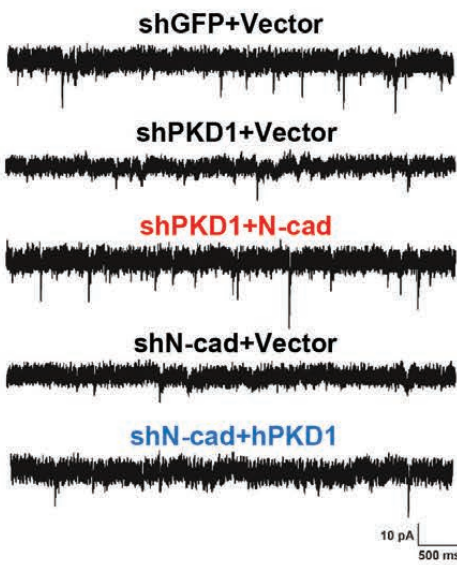
**B<sub>1</sub>**



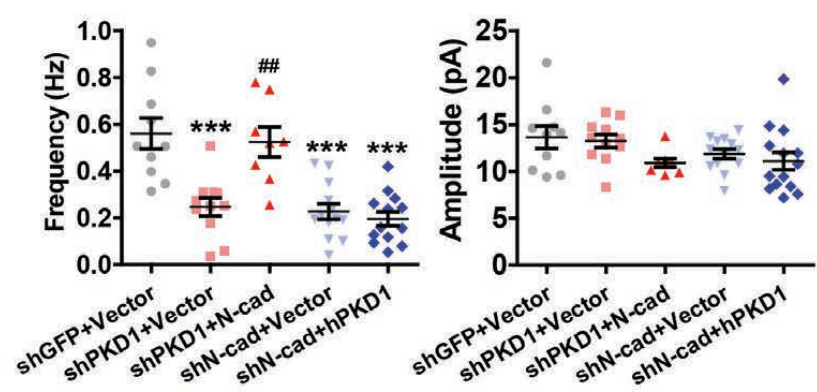
**B<sub>2</sub>**

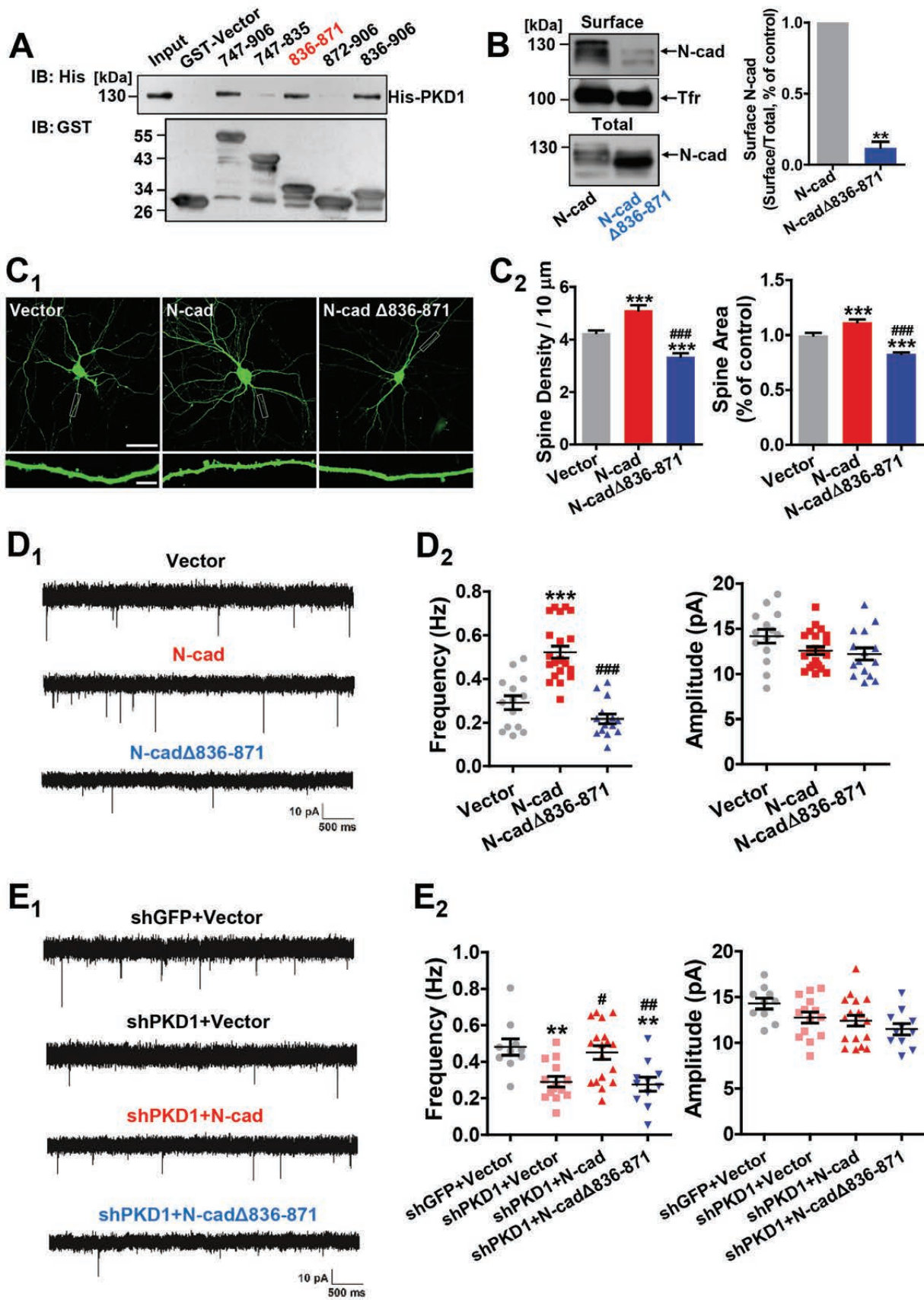


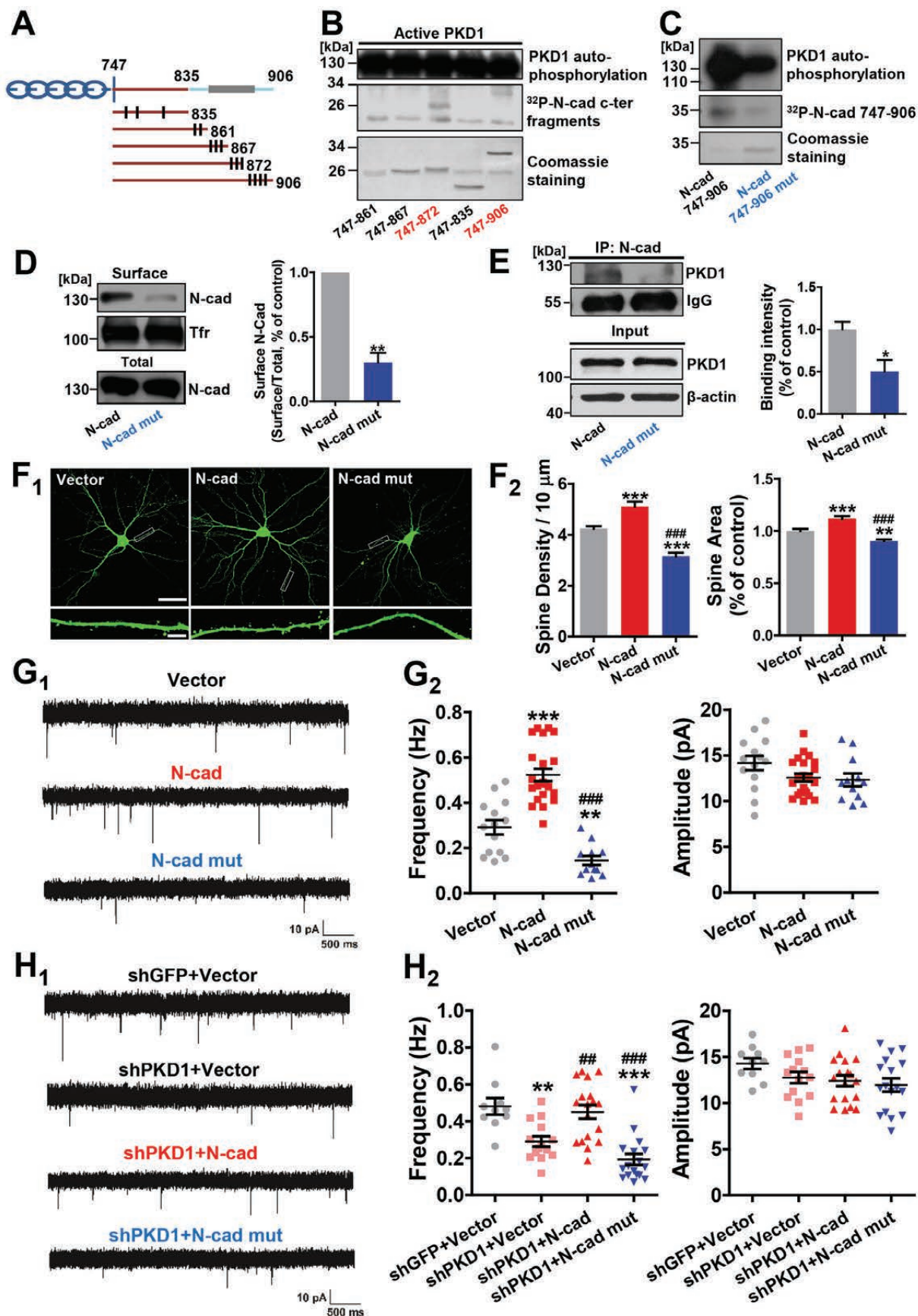
**C<sub>1</sub>**

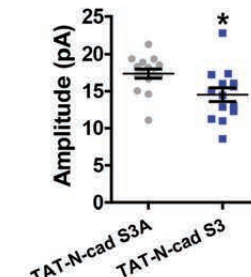
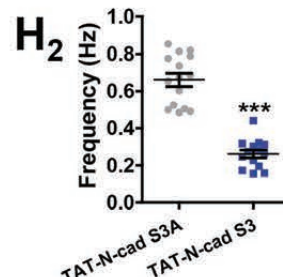
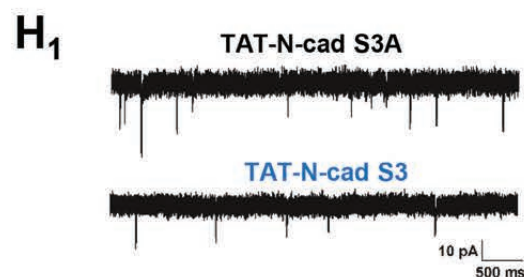
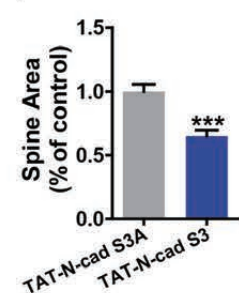
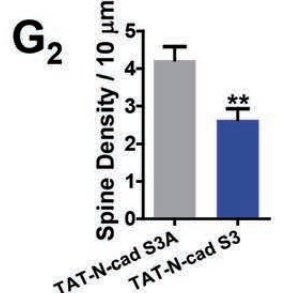
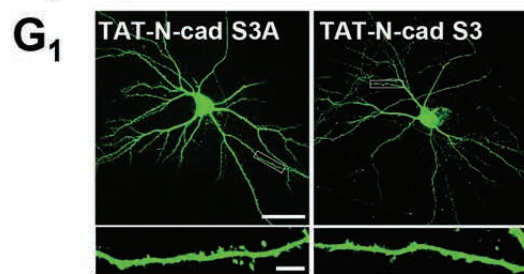
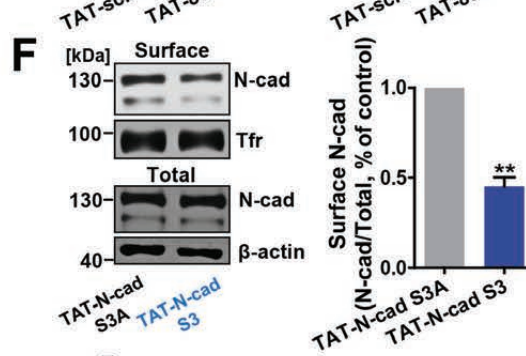
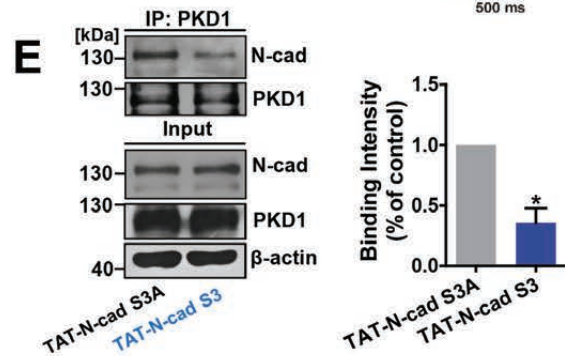
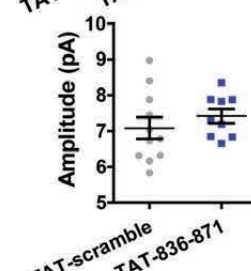
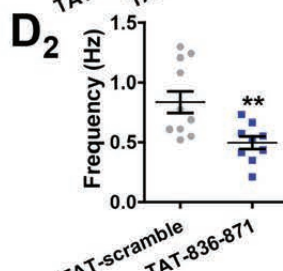
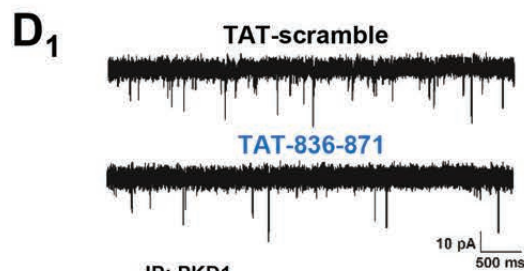
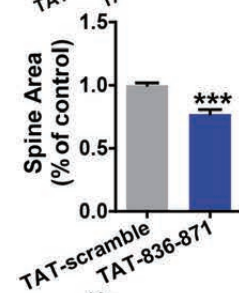
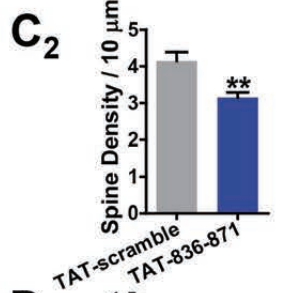
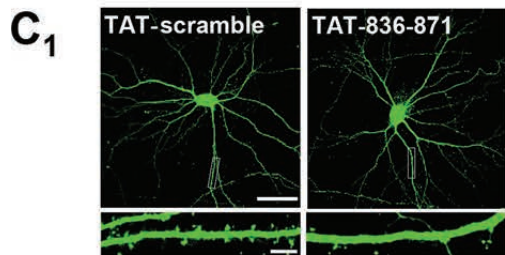
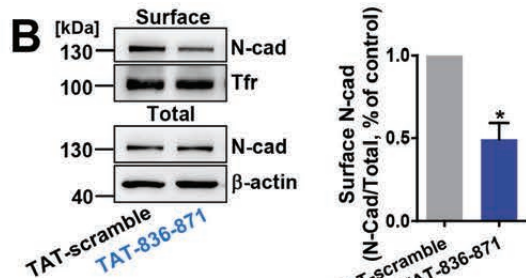
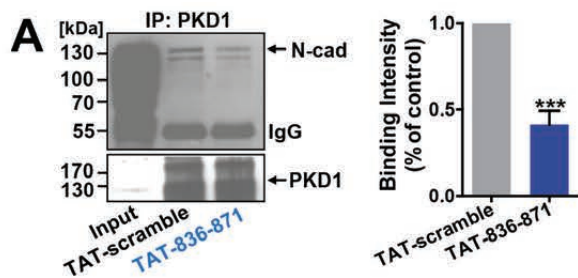


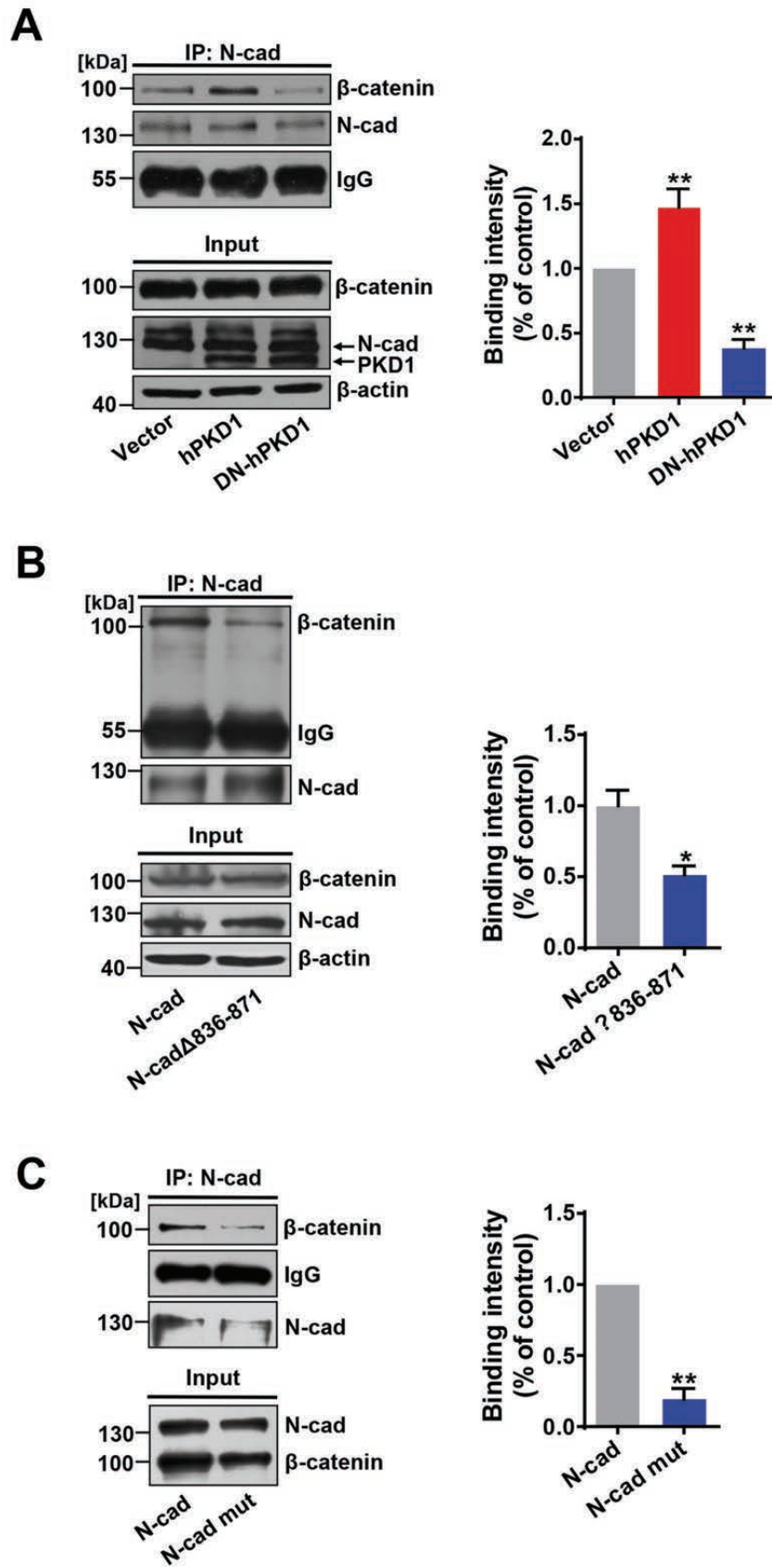
**C<sub>2</sub>**

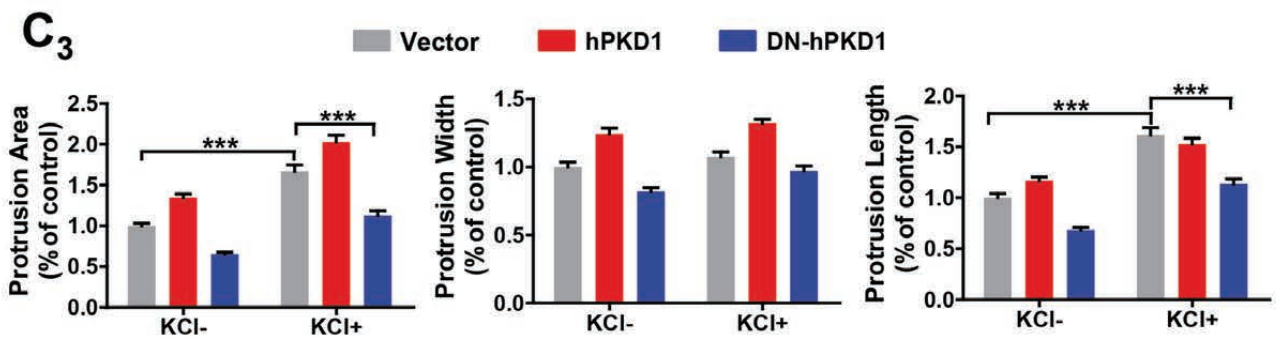
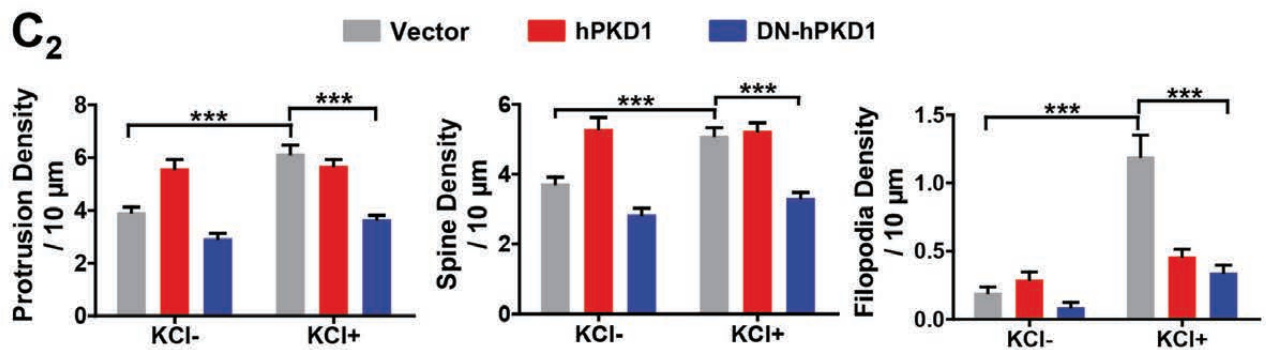
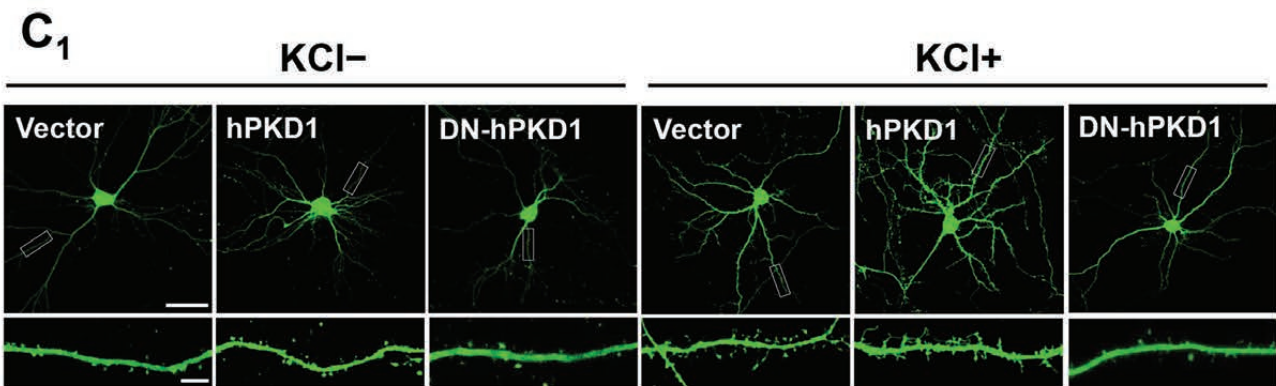
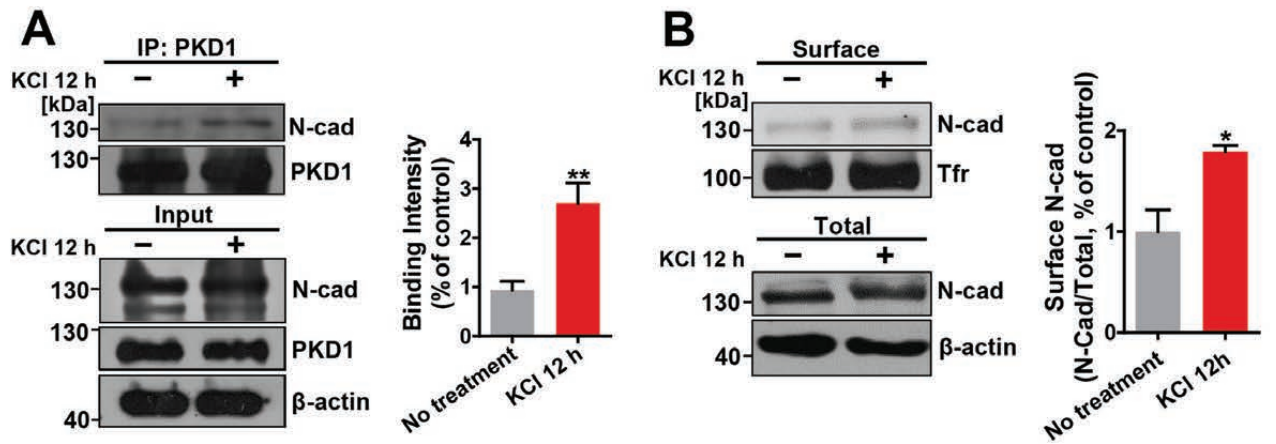


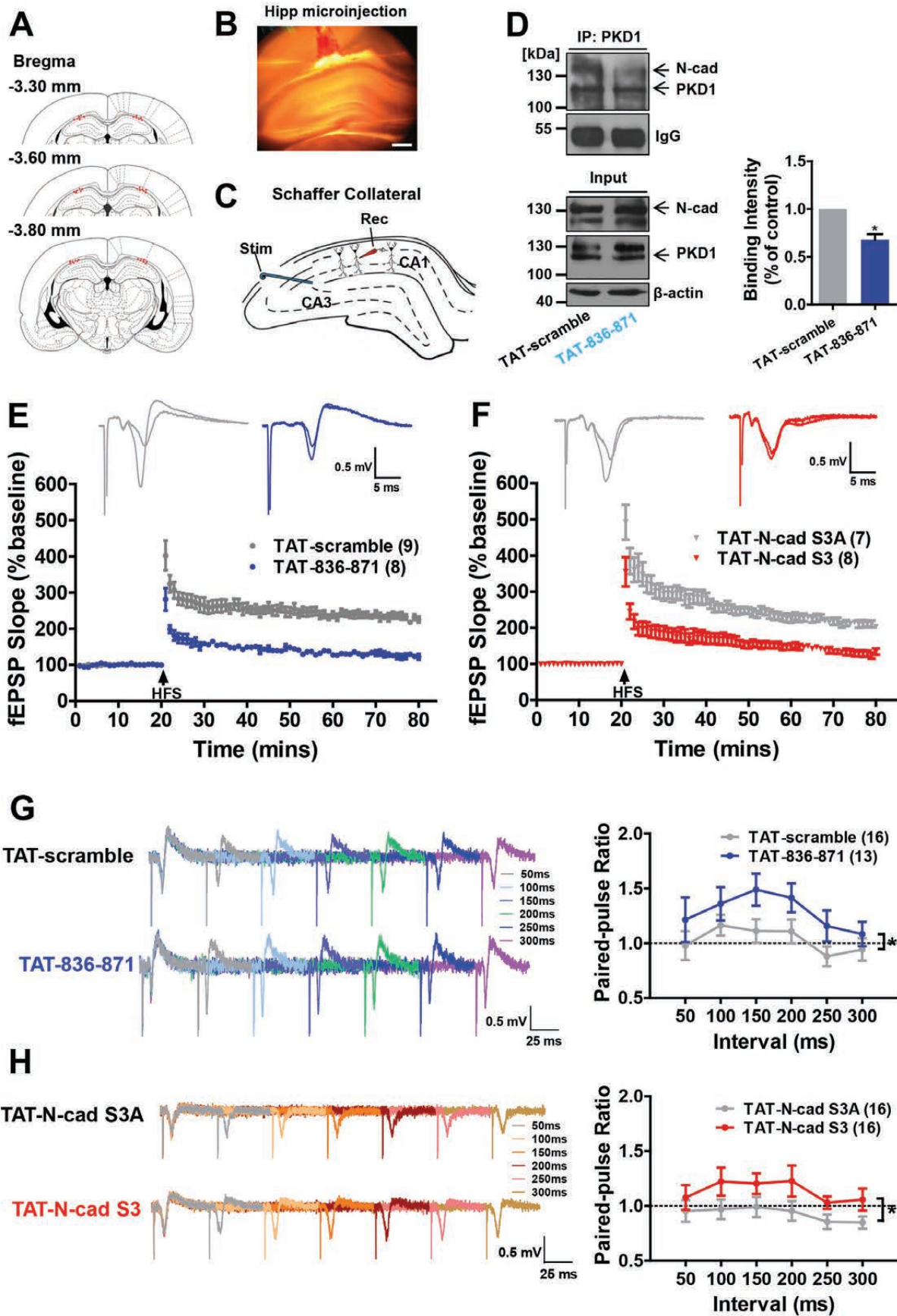












## Working Model

